2020

Sound propagation in viscous flows using piezoelectric sensors and non-destructive propagation techniques and its applications

ahmed M. abdulkareem

Sound propagation in viscous flows using piezoelectric sensors and non-destructive propagation techniques and its applications

A dissertation submitted in partial fulfillment of the requirements for the degree of Doctor of Philosophy at Virginia Commonwealth University

By

Ahmed Mohammed Abdulkareem

M.Sc. Mechanical Engineering, Al-Nahrain University, Iraq, 2000

B.Sc. Mechanical Engineering, Al-Nahrain University, Iraq, 1997

Director:

Dr. Karla Mossi
Associate Professor
Graduate Program Director
Department of Mechanical and Nuclear Engineering

Virginia Commonwealth University
Richmond, Virginia
June 2020

Acknowledgments

In the name of Allah, the Most Merciful and Beneficent

First and foremost, all praises and thanks are due to Allah, Almighty, the greatest of all, on whom we ultimately depend for sustenance and guidance. I would like to thank and praise Allah Almighty for giving me the opportunity, determination and the strength to finish this journey. His continuous grace and mercy have been with me throughout my life and ever more during the tenure of my research. I would like to thank God Almighty for enabling me to undertake this research study while giving me the perseverance to complete it satisfactorily. Without his blessings, this achievement would not have been possible.

No words can adequately express my sincere gratitude to my advisor, Dr. Karla Mossi, for her continuous support, guidance and encouragement. Additionally, I would like to thank committee members, Drs. Robert Saxton, Ibrahim Guven, Ravi Hadimani, and Ugur Erturun for their insightful comments, informative discussions and various perspectives, which helped motivate me into broadening my research boundaries.

I am, also, deeply indebted to Professor Gary Tepper for his useful guidance, unparalleled instruction and valuable training, which I found necessary in pursuing my degree.

More importantly, special thanks to the Higher Committee of Educational Development in Iraq (HCED) for their financial support and cooperation that assisted me during this endeavor.

Finally, none of this would have been to succeed without the constant source of love, patience, support, and motivation of my wonderful mother, my sisters, my brother, my two boys and my friend Odai Bani Mostafa.

Table of Contents

List of Tables

List of Figures

Abstract

Structural non-destructive evaluation techniques are applied to viscous flows to detect fluid property changes. The main operating principle consists of an actuator which provides a stimulus, and a sensor to receive a signal traveling to a fluid domain. The main challenge of the operating principle consists of investigating waves traveling in a viscous flow. Traveling waves utilizing a piezoelectric actuator-sensor pair are modeled and the results are validated experimentally. ANSYS models, coupled with a two-way fluid-solid interaction model, are built to investigate how far a signal travels and what frequency ranges are of interest. The numerical model includes modeling three different geometries (square, circular, triangular) for the actuator-sensor pair manufactured with three different piezoelectric materials (PZT4, PZT5A, PMN32). Numerical work is validated with experimental work using a pair of circular actuator-sensors manufactured with PZT5A and immersed in a large container of water and glycerin. Furthermore, in order to establish mesh independence of the results, three mesh refinement levels (coarse, medium and fine) were utilized with different materials, geometries and fluid viscosity values.

The actuator receives a 0.5 VAC signal ranging from 100 Hz to 40 MHz. The sensor records the signal at varying distances from the actuator, and the result is labeled as the gain or the ratio of received to send wave magnitude. The pattern of decay for both numerical and experimental results are in close agreement (the numerical decay are 10.825 and 11.4 for water and glycerin, respectively, while the experimental are 11.254 and 14.48 for water and glycerin, respectively). Numerically, the results show that the maximum acoustic pressure can be obtained by using a square piezoelectric actuator- sensor pair fabricated with PMN32. Numerically, the

results show that the maximum acoustic pressure can be obtained by using a square piezoelectric actuator- sensor pair fabricated with PMN32.

A viscosity probe for medical applications is developed using a piezoelectric actuator-sensor pair. The design constraints were size and cost. The actuator-sensor pair is manufactured with PZT5A with a rectangular shape to fit a 3 mL vacutainer. The actuator is excited by 0.5 VAC sinusoidal waves with varying frequencies ranging from 100Hz to 40 MHz. The sensor will detect the produced wave in the fluid. Also, the phase shift is recorded for different concentrations of glycerin and water to simulate different viscosities ranging from 1 to 1600 cP. The numerical analysis, a modal analysis, of the probe was performed and the results showed that the first, second and third modes of the device were in the range of 684–2358 Hz for air, 500–1080 Hz for water, and 469–625 Hz for glycerin. From the harmonic acoustic analysis, the results showed that the highest phase shifts, and maximum gain, occurs at the ultrasonic frequency range, 6 to 9 MHz. Hence, there is no relation between the natural frequencies of the probe and the ultrasonic frequency for the phase shift. Most importantly, a correlation between the phase shift and viscosity is found, making the probe a feasible device for measuring viscosity in an inexpensive, small, and disposable way.

CHAPTER 1

1.1 Background

Non-destructive evaluation (NDE) methods are widely used for structural health monitoring (SHM) of civil structures including bridges, dams and nuclear power plants [1]. Among them, wave propagation-based methods are commercially available and can detect failures of solid materials such as metals and composites, that have been used for over 20 years [2]. Piezoelectric based sensors are often utilized in the NDE systems, based on the piezoelectricity effect, which is defined as a generating of an electrical voltage across the piezoelectric material due to the applied stress or strain. The common material used in the sensors is Lead (Pb) Zirconate (Zr) Titanate (T) or PZT. PZT-based sensors are becoming more prevalent when compared with other sensors because of their monitoring performance and low-cost [3,4]. Piezo-based NDE methods include ultrasonic guided waves (UGW) with materials including polyvinylidene fluoride (PVDF) multielement sensors, macro fiber composite (MFC) sensors, and surface acoustic waves (SAW) PZT materials [5, 6]. In a typical wave propagation approach, applying an electric signal to the piezo-transducer generates waves that transverse the structure and are captured by the piezo-receiver [7]. The received signal should remain the same as long as the structural region between the transmitter and the receiver remains in good condition; if the structure defects, then the received signal will be changed. When changes (cracks, corrosions, e.g.) arise in the structure, a contrast between the previously recorded signals and the currently read signal may display.

Depending on the application, the ranges of ultrasonic wave frequencies can vary. For instance, in biomedical ultrasound applications, the required resolution is on the micrometer scale, which requires operating frequencies over tens or hundreds of megahertz [8]. Other applications, like marine transmission, require a frequency range of less than 10 kHz. In this case, optical fibers

are used and have played an essential role over the last 20 years as an alternative to the existing piezoelectric materials because of their high sensitivity and ability to minimize electromagnetic interference [9-25]. Ultrasonic waves have been an integral part of industry and research in recent decades [26]. One application of ultrasonic waves is the detection of internal defects in sound conducting materials. In this case, a short pulse generated by an electric charge is applied to a piezoelectric crystal. This crystal will vibrate for a very short period at a frequency related to the thickness of the crystal. The frequency for detecting a flaw is usually performed in the range of 1 MHz to 6 MHz. At this frequency range, the vibrations or sound waves have the ability to travel at significant distance in homogeneous elastic materials. For instance, K. Kwong, et al [27], monitors hydration in structures based on the Surface Wave Propagation (SWP) technique. This technique is based on measuring mechanical properties of the structure such as dynamic Young's modulus and compressive strength of concrete.

Other work detected cracks or damage in bolts or joined steel bridge components. The detection of cracks or damage in the structure can be monitored using PZT patches attached to the structure to detect the growth of cracks in the bridge components [28, 29]. Song, et al [30], present a numerical simulation and experimental setup to investigate the wave propagation mechanism in honeycomb sandwich structures using PZT actuators/sensors. The results showed that the global guided waves in the composite can be detected when loading frequency is low. Experimental testing was performed to validate the numerical results. Very good agreement is noticed between the numerical and experimental results. V. Chillara, et al [31], investigate the change of the load and temperature on a guided wave third harmonic generation from shear horizontal (SH) waves in aluminum plates. Magnetostrictive transducers were used to excite the shear horizontal waves (SH) and a measurement of third harmonic was made under increasing static – tensile loads at a constant

temperature. Song, et al [32], developed a numerical simulation to investigate the surface wave generation and reception using a pair of piezoelectric actuators/sensors and the numerical model ran at higher frequency range cases. The results obtained examined some features of the microstructure effects on the surface wave propagation. Also, an experimental test was conducted to validate the numerical simulation. The results obtained include velocity dispersion curves of the surface waves. Those curves are important for the future damage detection in concrete materials. The results show a good agreement for the potential and feasibility of using piezoelectric actuators/sensors to generate and receive surface waves for damage detection in concrete structures.

These non-destructive techniques may be quite useful for the determination of fluid properties. Fluids are found everywhere and serve a vital role in a wide range of processes, from machinery to the human body [33,34]. Regardless of the area, it is always helpful, or even required, to monitor the specific condition of the fluids. For instance, online measurement of the fluid properties is an essential task for machinery [35] or human body health monitoring [36]. Young's modulus, conductivity, permittivity, density, and viscosity are essential parameters for evaluating the status of the fluid through physical sensing. Among them, viscosity can be considered as the most significant physical property because it regulates and determines the shear stress/shear rate interaction of the fluid. In other words, viscosity quantifies the resistance to the flow of a fluid and plays an important role in the field of rheology. Fluids conforming to Newton's linear law of friction are known as Newtonian fluids (e.g., air, water, simple oils), and they demonstrate a linear correlation between shear stress and shear strain rate [34-37]. Non-Newtonian fluids do not follow this linear law and exhibit more complicated shear stress to strain rate behaviors due to their

complex molecular structures (e.g., polymers, blood). These fluids are generally highly viscous, and measurement of their properties is more complicated compared to Newtonian fluids.

In order to determine the properties of a fluid, it is useful to know the speed of pressure wave propagation, which is identical to acoustic velocity and determined by the density and mass-to-pressure derivative of the bulk modulus of the fluid. Since it is crucial to quantity for the fluid characteristics, researchers have developed methods and predictive models to obtain accurate acoustic velocity data in different fluids, including oil, biodiesel fuel, water, glycerin e.g., at various pressures and temperatures [38-40]. Vance and Brown [41], reported the acoustic velocity in the water at room temperature to be about 1500 ms^{-1}. Besides, E.S. Jeon et al [42], used an acoustic inspection method based on ultrasonic sensors to measure the acoustic velocity in glycerin as a function of temperature, and recorded it at room temperature around 1900 ms^{-1}. The ultrasound cell method, based on two ultrasonic transducers, where one served as a transmitter and the other as a receiver, is one of the most common methods for acoustic velocity measurements. In this approach, the transmitter generates acoustic waves that propagate across the test fluid, and the receiver collects them. Then, by using the difference between the transmitter-receiver propagation time and the distance between the transducers, acoustic velocity data can be calculated.

Applying a non-destructive evaluation to fluids and exploring the behavior of fluid properties becomes more important in different fields such as aerospace, medicine, chemistry and biology fields [43]. The ultrasonic transducer is one of the most important devices in the NDE system. S.Banerjee et al [44], developed a technique to calculate the ultrasonic field (pressure and velocity) generated by ultrasonic transducers. This technique is based on the distributed point source method (DPSM), which mainly includes a model of the ultrasonic field generated in a multilayered nonhomogeneous fields system. Two different cases have been considered. The first

case is a geometry problem with three layers of nonhomogeneous fluid, while the second case contains four layers of nonhomogeneous fluid. In both cases, an excitation with different frequencies has been implemented at different orientations of the transducers. The results showed that the ultrasonic field is very sensitive to the fluid properties.

All these methods to detect damage in a structure, can be extended to liquids. For instance, non-destructive, low-cost systems are increasingly required to evaluate the viscosity of fluids in real-time. This method can be used on Lab-on-chip (LOC) devices to perform several laboratory analyses with high precision [45,46]. These devices can be used in different applications in biological, chemical and physical research. They work by creating a standing acoustic wave generated by a pair of opposite actuators obtaining pressure nodes in fluids [47-50]. The forces generated by the integration between the acoustic waves and fluids can be used to separate the fluid from the particles. N. Orloff et al [50], designed a surface wave resonator with microfluidics to manipulate particle trajectories. The resonator has the ability to change the position of the acoustic nodes by changing the electronic phase of the transducers relative to the other in a pseudo-static manner. Demori M et al [51], fabricated a device to generate acoustic modes based on Flexural Plate Waves (FPW). These waves can be generated using Lead Zirconate Titanate (PZT) as actuators attached to Interdigital Transducers (IDT) printed on alumina (AL_2O_3) substrate. This device can separate the particles from the fluid by the standing waves generated by the PZT actuators at a resonance frequency. This device can separate the particles from the fluid by the standing waves generated by the PZT actuators at a resonance frequency.

Also, the non-destructive evaluation technique has been used for monitoring fluid properties such as density and viscosity. Antlinger et al [52-55], used a non-destructive concept by using pressure waves to detect the acoustic impedance characteristic of a fluid. In a comprehensive study

[52], they demonstrated that the fluid-solid relationship influences the wave propagation properties of a PZT device. Their research further recorded the electrical impedance of PZT resonators in a number of fluids with varying viscosities, demonstrating that the amplitude of the impedance increases as the material becomes less viscous or vice versa. They proved that electrical impedance, which is a component of fluid parameters (speed of sound, viscosity, and damping, e.g.), influences the resonance frequencies for a sensor surrounded by the fluid, under an excitation voltage. R.Waxman et al [56], used a pre-stressed (PZT) probe to monitor a change in viscosity. This probe consisted of a paired actuator-sensor, where the actuator was excited by a voltage of 1 V_{RMS}, and the sensor received a vibration wave and turned the wave into an output signal. Measurements of gain and phase of the vibration wave, through the fluid medium, were recorded and analyzed. The results showed that the viscosity varies exponentially with the resonance frequency of the probe measured by the impedance analyzer. Abdulkareem et al [57], built an inexpensive and disposable device for measuring fluid viscosity based on the non-destructive evaluation technique. The design incorporates a sensor/actuator pair using a piezoelectric material layered with copper/brass and is capable of monitoring viscosity changes in low volume liquids (e.g.,vacutainer vial). Experiments performed with the new device show a definite pattern of wave propagation in viscous solutions. A numerical model is built to investigate the wave propagation in the fluid. For experimental measurements, the sensor part of the device detects the generated pressure wave in fluid (e.g., air, water, glycerin) by the actuator part. The phase shift between the actuator and the sensor signals is then recorded and plotted for different concentrations of glycerin and water at room temperature. The results of this study show a direct correlation between the phase shift and varying viscosity in the ultrasonic frequency range from 6 to 9 MHz. The numerical simulation, performed utilizing acoustic modal and harmonic response analysis, results also

demonstrate the same trend as the experimental results: a phase shift increases with the viscosity of the fluid.

1.2 Motivation

Due to the increasing need to monitor fluid properties, such as viscosity, quickly and efficiently in process flow (manufacturing or processing industries) or with minimal sample size (medical industry), there is a need to investigate non-destructive techniques on fluid properties. This work addresses the needs and develops an application by fabricating a device that can have a significant effect on the healthcare industry.

1.3 Goal

The goal of this work is to demonstrate that non-destructive evaluation techniques can be applied to monitor a fluid property such as viscosity using ultrasound wave propagation. This work includes numerical and experimental investigation on wave propagation of an actuator-sensor pair to be used for the non-destructive evaluation of the Newtonian fluid properties. First, the effect of varying distance between the actuator and sensor was studied. Then, different commercially available piezoelectric materials (PZT-4, PZT-5A, and PMN-32) with varying geometries (square, circular, and triangular) were modeled to assess their effects on wave propagation in a fluid. This analysis was performed numerically and validated experimentally. The numerical analysis included a derivation of the mathematical formulation based on Fluid – Structural Interaction (FSI) techniques applied between the actuator-sensor pair and the surrounding stationary fluid. This method included a solution of the dynamics equation for the structure coupled with the continuity and Navier-Stokes equations for the fluid domain. Three-dimensional models were built using SolidWorks® software. The numerical analysis included performing a harmonic analysis for the actuator under applied sinusoidal excitation voltage. Next, the transferred data from this analysis

to the fluid domain occurred by performing a harmonic acoustic analysis and finally, performing another harmonic analysis to the sensor. These results were then validated experimentally. The second main objective was to develop an application for the healthcare industry. In this case, an actuator-sensor pair was coupled to a beam that can be immersed in a fluid in a 3ml vacutainer. Experimental and numerical simulations were performed to optimize the results.

To validate the model, an experiment was designed using a circular actuator-sensor pair attached to a holder and immersed into a container filled with a fluid. The sensor can displace a certain distance from the actuator to match the numerical modeling. The experiment includes a measurement of the signal sent and received. Using the described approach, an actuator-sensor pair is designed to monitor changes of viscosity in a water/glycerin mixture in a small 3ml vacutainer. These particular containers are used to obtain blood samples of patients in the healthcare field.

1.4 Unique Contributions

The main contributions are in the field of non-destructive evaluation technique in liquids; this technique can be used for monitoring fluid properties using the same principles of wave propagation in solid structure. In this case, an acoustic wave travels through a viscous flow and changes throughout the liquid are simulated and measured. These changes are correlated to the properties of the fluid.

1.5 Dissertation Outline

To address the main goal, the dissertation is divided into **Six chapters** via the following outline:

Chapter 1 gives the general introduction about the non-destructive evaluation method and their applications in the solid, ultrasonic frequency ranges of the non-destructive method and its applications in the fluid.

Chapter 2 includes the mathematical formulation derivation for the actuator / sensor pair and the attached structure and its surrounding fluid. It also contains the experimental setup for the piezoelectric immersed in the fluid and create a numerical model to be matched with the experiment for both solid and fluid with proper dimensions using SolidWork. Mechanical properties for the materials device were selected, mesh configurations for both fluid and solid were assigned, boundary conditions to the structure were applied to be consistent with the experiment and finally, a harmonic and acoustic harmonic analysis for both solid and fluid based on the Two-way Fluid Structure Interaction was performed.

Chapter 3 includes the results and discussion for the experimental setup and numerical simulations.

Chapter 4 describes the design, fabrication and numerical and experimental investigation for a device based on non-destructive evaluation for measuring fluid viscosity based on the optimal design and selection from the experimental and simulation results from chapter 2 and 3.

Chapter 5 summarizes the conclusions and the outcomes of this dissertation study.

Chapter 6 explores the challenges and recommendations for future work.

CHAPTER 2 Fluid-Structure Interaction (FSI) and Numerical Modeling

Fluid – Structure Interaction (FSI) problems can be described as one or more solid structures immersed or surrounded by a fluid. FSI problems have significant effect for the analysis in many engineering fields [58]. The nonlinearity and multidisciplinary of different engineering fields become a challenge to find analytical solutions to the model equations. In addition, performing experiments are limited and expensive for some engineering problems; therefore, numerical simulations can be applied to investigate the complex interaction between the fluid and solid [59-61].

With the developments of computer technology, simulations of the engineering system become increasingly required and complicated. Therefore, an efficient numerical algorithm can be used to investigate the interaction between structure and fluid domain. Examples of different FSI applications include but not limited to, is the particle assembly [62], aerodynamics [63, 64],turbulence [65, 66],complex flow in irregular domain [67-69],electro-hydrodynamics flows [70], magneto-hydrodynamic flows [71], biofluid and biomechanics (such cell aggregation and deformation ,blood – heart interaction, inner ear fluid dynamics) [72, 73].

In this chapter, all the details of the Fluid Structural Interaction (FSI) mathematical derivation and formulation are described. Also, the numerical simulation for the sensor and actuator (Structure), and the fluid domain based on the FSI method is detailed. The numerical simulation has been done using Finite Element Analysis (FEA) through ANSYS and Solid Works.

2.1 Fluid Structure Interaction (FSI)

To take into consideration the effect of the fluid domain surrounded by the vibrating beam, the system has to be set up as a Fluid Structure Interaction (FSI) problem. The FSI method combines the solid structure of the vibrating beam with the fluid domain to capture the interaction

between the effect of vibrating solid structure on the fluid domain. In this method, the FSI is mainly based on the solution of the equation of motion for the structure under applied load (excitation voltage in this case), coupled with the equation of motion for the fluid. This model can be described by coupling the equation of motion of the structure and the equation of motion of the fluid. The discretized equation of motion of the structure can be written as [74]:

$$[M_s]\{\ddot{u}\} + [C_s]\{\dot{u}\} + [K_s]\{u\} = \{F_s\} \tag{2.1}$$

Where [Ms], [Cs], [Ks], {Fs}, and {u} are the structural mass, the structural damping, the structural stiffness matrices, the applied load and nodal displacement vectors, respectively. To model the fluid–structure coupling, the behavior of the fluid pressure can be described with acoustic wave equation. This behavior can be derived from continuity equation of motion, with Navier–Stokes equation of motion described below with the following assumptions [75, 76]:

$$\nabla . \vec{V} = 0 \tag{2.2}$$

$$\rho \frac{D\vec{V}}{Dt} = -\nabla p + \rho \vec{g} + \mu \nabla^2 \vec{V} \tag{2.3}$$

Total derivative Pressure gradient Body force term Viscous term

(a) the fluid is compressible (density changes due to pressure variations), (b) the viscous dissipation term in the Navier–Stokes equation is neglected, (c) the flow is irrotational, (d)body force is neglected (e) no mean flow of the fluid, and (f) changes of the mean density and pressure remain small in different areas of the fluid domain.

By applying the above assumptions on Navier-Stokes equation and the continuity equation, the coupling leads us to Helmholtz's equation:

$$\nabla^2 P = \frac{1}{c^2}\frac{\partial^2 P}{\partial t^2} \tag{2.4}$$

where P is the fluid pressure; c is the speed of sound, t is the time, and ∇^2 is the Laplacian operator.

The Helmholtz's equation represents the equation for the wave propagation in the fluid, taking into consideration that the viscous dissipation will be neglected. The Helmholtz's equation can be described in matrix notation by introducing a matrix {L} operator as shown in equation 2.5:

$$\frac{1}{c^2}\frac{\partial^2 P}{\partial t^2} - \{L\}^T(\{L\}P) = 0 \tag{2.5}$$

Then, the discretized Helmholtz's Equation using a Galerkin method, as described in the literature [77], is shown in equation 2.6, where *vol* is the volume of the domain, $\delta P = \delta P(x,y,z,t)$, S is the surface, and n is the normal to that surface [78].

$$\int_{vol}\frac{1}{c^2}\delta P\frac{\partial^2 P}{\partial t^2}d(vol) + \int_{vol}(\{L\}^T\delta P)(\{L\}P)d(vol) = \int_s\{n\}^T\delta P(\{L\}P)d(S) \tag{2.6}$$

In addition, the fluid momentum equation yields equation 2.7 which highlights the normal pressure gradient of the fluid and the normal acceleration of the structure at the fluid-structure interface S [78].

$$\{n\}\cdot\{\nabla P\} = -\rho_0\{n\} \tag{2.7}$$

The derived equation for the fluid pressure gradient, and the structure acceleration at the fluid-structure interface, is shown in equation 2.8, where U is the displacement vector, and ρ_0 is the mean fluid density [79, 80]. equation 2.8 represents the combined derived equation, and the discretized modified Helmholtz's Equation.

$$\int_{vol} \frac{1}{c^2} \delta P \frac{\partial^2 P}{\partial t^2} d(vol) + \tag{2.8}$$

$$\int_{vol} (\{L\}^T \delta P)(\{L\}P) d(vol) = \int_s \rho_0 \delta P \{n\}^T \left(\frac{\partial^2}{\partial t^2} U\right) d(S) - \int_s \delta P \left(\frac{\beta}{c}\right) \frac{\partial P}{\partial t} d(S)$$

The finite element shape functions for spatial variation of the fluid pressure P, and the structural displacement U, are defined in equations 2.9 and 2.10.

$$P = \{N_p\}^T \{p\} \tag{2.9}$$

$$U = \{N_u\}^T \{u\} \tag{2.10}$$

The finite element statement is defined by the Helmholtz's Equation, where $\{N_p\}$ the element shape function for pressure, $\{N_u\}$ is the element shape function for displacements, $\{p\}$ is the nodal displacement component vectors, and $\{u\} = \{u_x\}, \{u_y\}, \{u_z\}$ are the nodal displacement vectors, as shown in equation 2.11.

$$\int_{vol} \frac{1}{c^2} \{\delta p\}^T \{N_p\} \{N_p\}^T d(vol) \{\ddot{p}\} + \int_{vol} \{\delta p\}^T [B]^T [B] d(vol) \{p\} \tag{2.11}$$

$$+ \int_s p_0 \{\delta p\}^T \{N_p\} \{n\}^T \{N_u\}^T d(S) \{\ddot{u}\}$$

$$+ \int_s \frac{\beta}{c} \{\delta p\}^T \{N_p\} \{N_p\}^T d(S) \{\dot{p}\} = 0$$

$$where\ [B] = \{L\}\{N_p\}^T$$

and the matrix notation of Helmholtz's Equation is shown in equation 2.12.

$$[M_f]\{\ddot{p}\} + [C_f]\{\dot{p}\} + [K_f]\{p\} = \{F_{sf}\} \tag{2.12}$$

Where:

$$[M_f] = \frac{1}{c^2}\int_{vol} \{N_p\}\{N_p\}^T d(vol)$$

$$[C_f] = \frac{\beta}{c}\int_{s} \{N_p\}\{N_p\}^T d(S)$$

$$[K_f] = \int_{vol} [B]^T[B] d(vol)$$

$$[F_{sf}] = -p_0 \int_{s} \{N_p\}\{n\}^T\{N_u\}^T d(S)\{\ddot{u}\}$$

The coupling matrix representing the effective surface area of the fluid structure is shown in equation 2.13.

$$[R] = \int_{s} \{N_u\}\{N_p\}^T\{n\} d(S) \tag{2.13}$$

So that the simplified fluid load equation shown in Equation 2.14:

$$\{F_{sf}\} = -p_0[R]^T\{\ddot{u}\} \tag{2.14}$$

The structural dynamics equation for fluid pressure at the interface is shown in equation 2.15:

$$[M_f]\{\ddot{p}\} + [C_f]\{\dot{p}\} + [K_f]\{p\} = \{F_s\} + \{F_{fs}\} \tag{2.15}$$

where the fluid load vector, $\{F_{fs}\}$:

$$\{F_{fs}\} = \int_s \{N_u\} P\{n\} d(S) = \int_s \{N_u\}\{N_p\}^T\{n\} d(S)\{p\} = [R]\{p\} \tag{2.16}$$

The complete finite element equation in discretized equation for the Fluid Solid Interaction problem can be written as shown in equation 2.17 and details can be found in [81].

$$\begin{bmatrix}[\mathrm{M_s}] & [0]\\ [\mathrm{M_{fs}}] & [\mathrm{M_f}]\end{bmatrix}\begin{Bmatrix}\{\ddot{u}\}\\ \{\ddot{p}\}\end{Bmatrix} + \begin{bmatrix}[\mathrm{C_s}] & [0]\\ [0] & [\mathrm{C_f}]\end{bmatrix}\begin{Bmatrix}\{\dot{u}\}\\ \{\dot{p}\}\end{Bmatrix} + \begin{bmatrix}[\mathrm{K_s}] & [K_{fs}]\\ [0] & [\mathrm{M_f}]\end{bmatrix}\begin{Bmatrix}\{u\}\\ \{p\}\end{Bmatrix} = \begin{Bmatrix}\{F_s\}\\ \{0\}\end{Bmatrix} \tag{2.17}$$

where, [Ms], [M_f], [C_s], [C_f], [K_s], [M_{fs}], and [K_{fs}] denotes the structural mass, the fluid mass, the structural damping, the fluid damping, the structural stiffness, the equivalent coupling mass, and the equivalent coupling stiffness matrices, respectively; and {F_s}, {u}, and {p} represents the applied load, the nodal displacement, and the acoustic pressure vectors.

Equation (2.17) represents the matrix mathematical formulation of the vibrating structure surrounded by the fluid domain. This equation can be used in this work by considering the actuator under an applied excitation voltage, and the sensor as a solid structure that vibrates due to the wave propagation for the fluid surrounding the solid structure.

2.2 Finite Element Simulation

The numerical simulation in this work includes modelling and investigation of acoustic pressure wave propagation. This model includes using three different types of actuator/sensor piezoelectric materials with three different geometries immersed in a container filled with a fluid. To this end, due to the complexity of the model, a common software, ANSYS® relase19R2, was used to investigate the acoustic waves generated by the excitation voltage applied on the actuator by using the Fluid Structure Interaction (FSI) method.

2.3 Actuator and Sensor

In this case the actuator and sensor were modeled always as a pair with the same dimensions, materials, and geometry. Within these parameters, the type of material used to create the actuator/sensor pair was evaluated: PMNPT or single crystal, PZT Type 5A and PZT type 4. These three materials were chosen for their different actuator/sensor properties, availability, and price. Additionally, three different geometries for the actuator/sensor pair were chosen: square, circular, and triangular. These shapes were utilized in noise cancelation and non-destructive evaluation applications. The model includes the holder for the actuator and the sensor assigning the mesh for both the structure and the surrounding fluid domain. Then appropriate boundary conditions were applied to perform a harmonic acoustic analysis for actuator/sensor piezoelectric pair immersed in a fluid. The model was created using a SolidWorks 2018® to design the actuator-sensor assembly, the wiring, and the surrounding fluid.

2.4 Experimental Setup

In order to test a non-destructive method in a liquid, a device was designed. This device consists of a large container with dimensions of 380 and 105 mm, such that the actuator and sensor are much smaller than the container and minimize wall effects. Holders were designed for the

actuator and the sensor, and wires are soldered directly to the device. First, a circular actuator/sensor pair was built and attached to a plastic holder as shown in Figure 2.2 (a), (b) and (c) which illustrates 3D models of the actuator/sensor pair immersed into a fluid. For the experiments only, a circular actuator/sensor pair was constructed using PZT Type 5A with a diameter and thickness 50.8 mm and 1.28 mm, respectively.

The built assembly consists of two circular PZT disks adhered to plastic holders with a conventional adhesive at room temperature. The assembly with the PZT, wiring immersed in a fluid is shown in Figure 2.1.

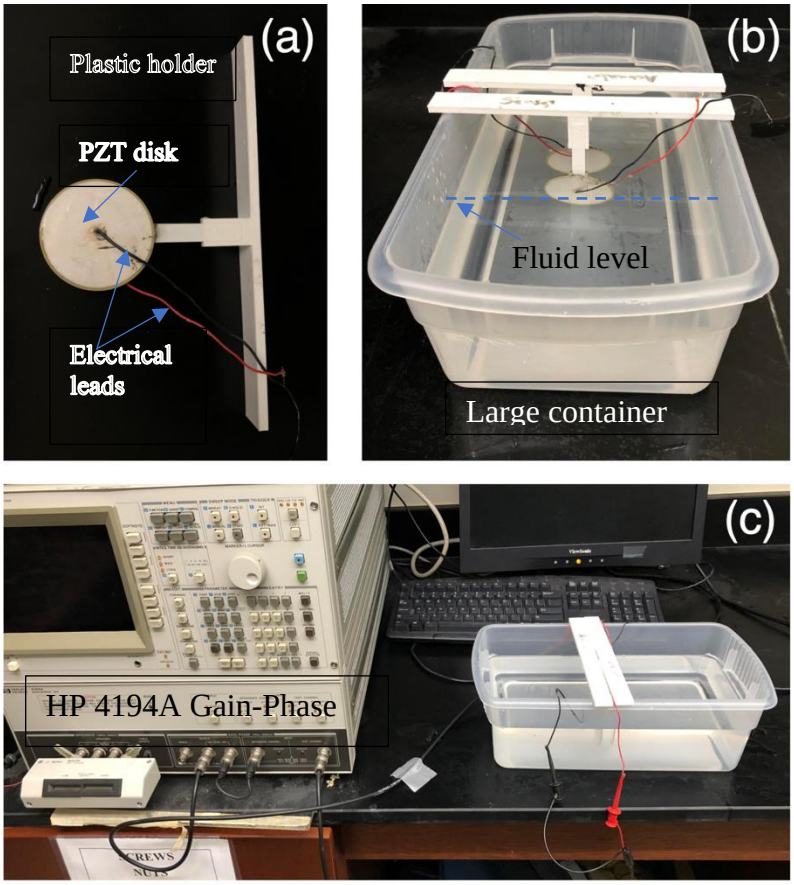

Figure 2.1 Testing setup; (a) actuator circular PZT5A attached to a plastic holder, (b) actuator/sensor pair immersed in a fluid, and (c) assembly connected to an impedance analyzer

In order to test the actuator/sensor piezoelectric pair in a fluid medium, a constant level of glycerin and distilled water were used. To minimize the effects of external factors on the results, fluid level, placement of the holder and temperature were kept constant throughout the experiments. The experimental setup, shown in Figure 2.1 was done by connecting the actuator to the input of the impedance analyzer and connecting the sensor to the output the analyzer. The impedance analyzer, a Hewlett Packard 4194A Impedance/Gain-Phase Analyzer was utilized to measure the voltage gain due to the excitation voltage applied to the actuator in a wide range of frequencies (100 Hz - 40 MHz, V_{in} = 0.5 V, High Impedance). In this manner, a signal was sent by the actuator and measured by the sensor in a variety of frequencies.

2.5 Numerical Model

The numerical model in this work includes creating the piezoelectric, plastic holder, fluid domain with proper dimensions to be consistent with experimental setup. SolidWork 2018® was used to create the model. The dimensions for the piezoelectric actuator/sensor pair can be tabulated in table (2.1):

Table 2.1 Dimensions of the piezoelectric actuator/sensor pair

Geometry	Piece #	Dimensions(mm)	Thickness(mm)
Circular	2	D=50.8	1.28
Square	2	H×W= (50.8*50.8)	1.28
Triangular	2	H×W= (50.8*50.8)	1.28

Figure 2.2 shows a schematic diagram for the assembly including the PZT, plastic holders, wires and the fluid domain.

(a)

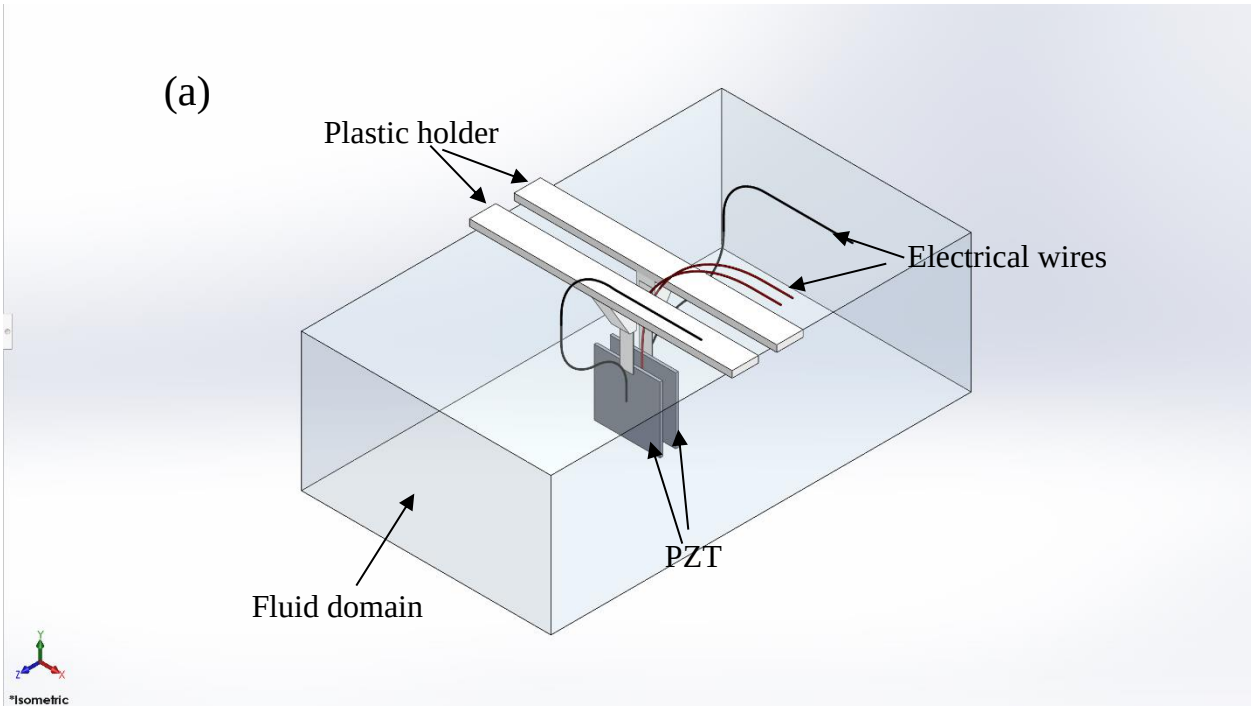

(b)

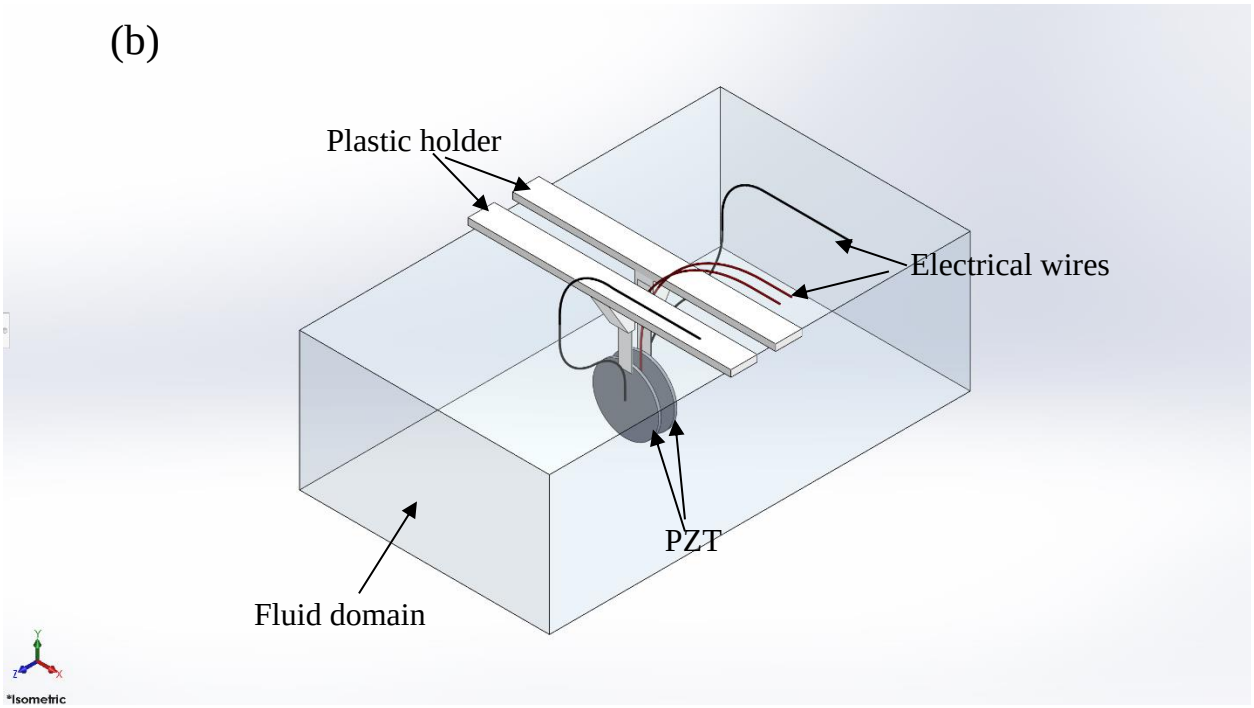

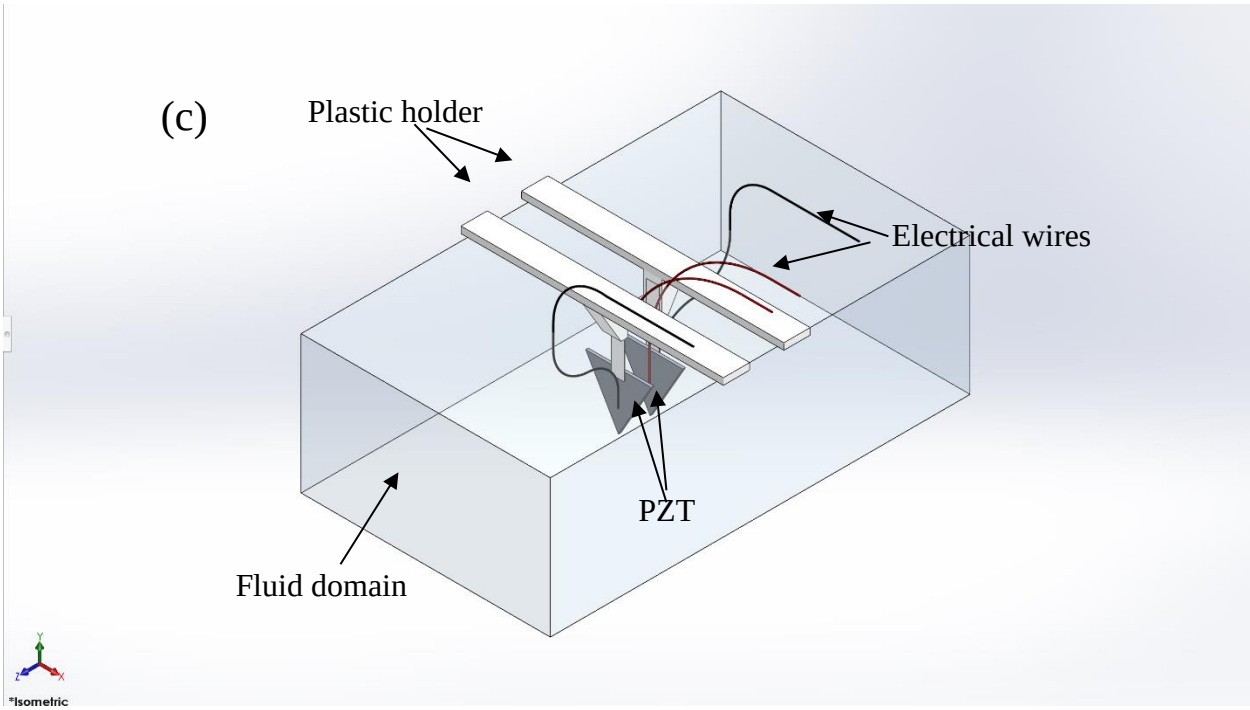

Figure 2.2 Assembly with (a) square (b) circular and (b) triangular actuator/sensor pair immersed in fluid

2.6 Materials

The mechanical properties for all types of piezoelectric materials and plastic holders used in the assembly can be shown in table (2.2), the material for the plastic holder is considered isotropic (i.e. the Modulus of elasticity for the material is constant). While, for piezoelectric materials, the material considered an anisotropic material (the modulus of elasticity for the materials is directionally dependent) [82].

Table 2.2 Mechanical Properties for the Assembly

Material	Piece #	Density (kg/m^3)	Modulus of Elasticity (N/m^2)
Plastic holder	2	925	2.7E+9
PZT 5A	2	7550	Appendix 1
PZT 4	2	7500	Appendix 1
PMN32	2	8040	Appendix 1

The piezoelectric material properties for the PZT are defined as [83]:

$$\left[\frac{\varepsilon}{\varepsilon_0}\right] = \begin{bmatrix} K_{11} & 0 & 0 \\ 0 & K_{11} & 0 \\ 0 & 0 & K_{33} \end{bmatrix} \tag{2.18}$$

$$[e] = \begin{bmatrix} 0 & 0 & e_{31} \\ 0 & 0 & e_{31} \\ 0 & 0 & e_{33} \\ 0 & 0 & 0 \\ 0 & e_{15} & 0 \\ e_{15} & 0 & 0 \end{bmatrix} \tag{2.19}$$

$$[\mathrm{C}] = \begin{pmatrix} C_{11} & 0 & 0 & 0 & 0 & 0 \\ C_{21} & C_{22} & 0 & 0 & 0 & 0 \\ C_{31} & C_{32} & C_{33} & 0 & 0 & 0 \\ C_{41} & C_{42} & C_{43} & C_{44} & 0 & 0 \\ C_{51} & C_{52} & C_{53} & C_{54} & C_{55} & 0 \\ C_{61} & C_{62} & C_{63} & C_{64} & C_{65} & C_{66} \end{pmatrix} \tag{2.20}$$

where [ε/ε$_0$] is the relative permittivity, [e] is the coupling (in C/m^2), and [C] is the elasticity matrices in (Pa), respectively.

2.7 Mesh type

The mesh element type of the actuator/sensor piezoelectric pair and the surrounding fluid domain were assigned automatically using mesh element Solid 186 for the sensor, while Solid 187 was used for the surfaces interacting with the fluid and the sensor, as shown in figure 2.3 a and b. Mesh element Solid 186 has a quadratic displacement behavior, and each node contains three orthogonal translational degrees of freedom, which ensures the mesh is accurate and complete. For the fluid surrounding the sensor, Fluid 220 was used for the fluid domain, while, Fluid 221 was utilized for the surfaces interacting between the fluid domain and the probe, as shown in figure 2.4a and b. Fluid 220 and Fluid 221 have four degrees of freedom: the pressure and three translational degrees of freedom [84].

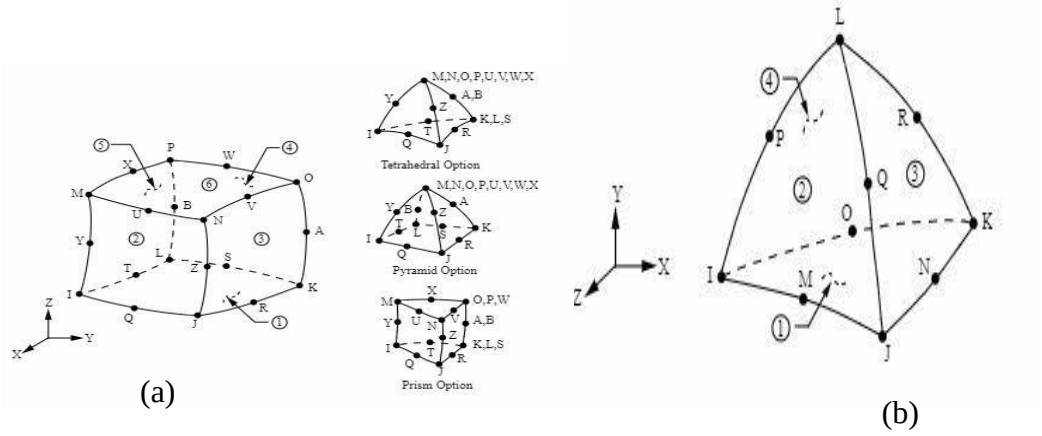

Figure 2.3 Mesh type for solid parts in the model (a) Solid 186 (b) Solid 187 [84]

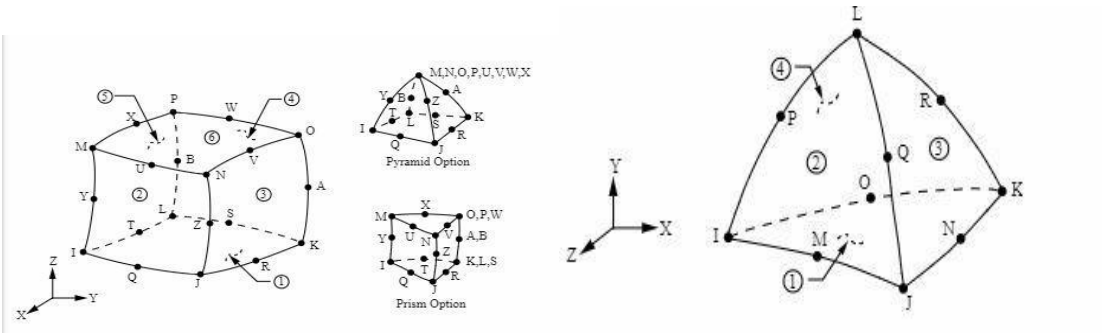

Figure 2.4 Mesh type for fluid parts in the model (a) Fluid 220 (b) Fluid 221 [84]

Figures 2.5a, b and c show a mesh configuration for the PZT assembly surrounded by a fluid for square, circular and triangular PZT pair, respectively.

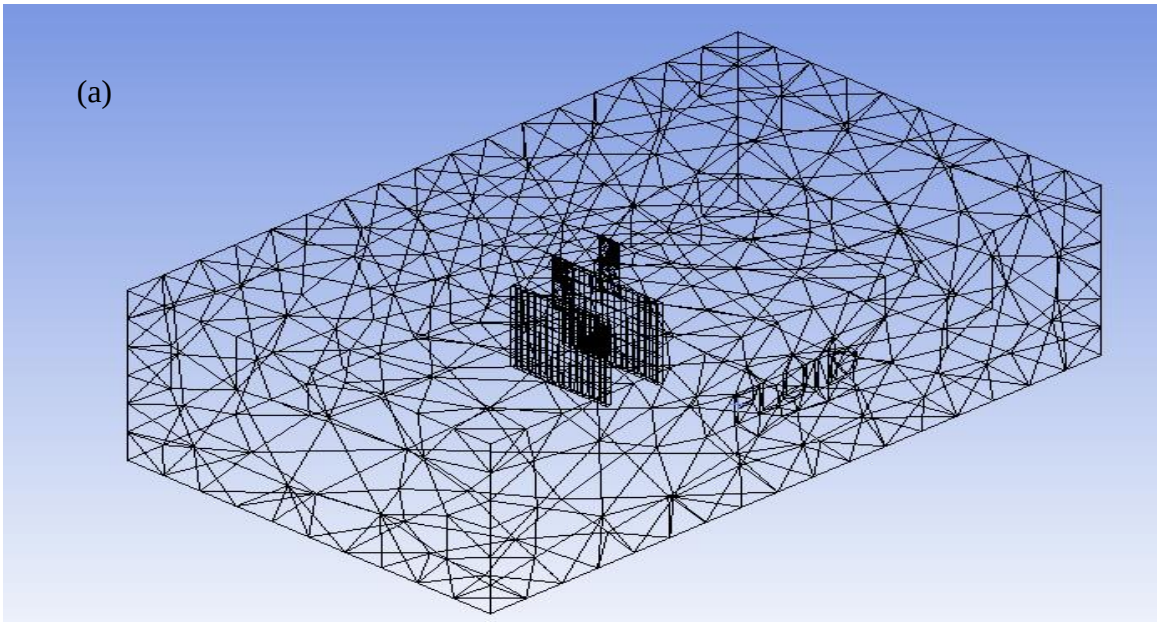

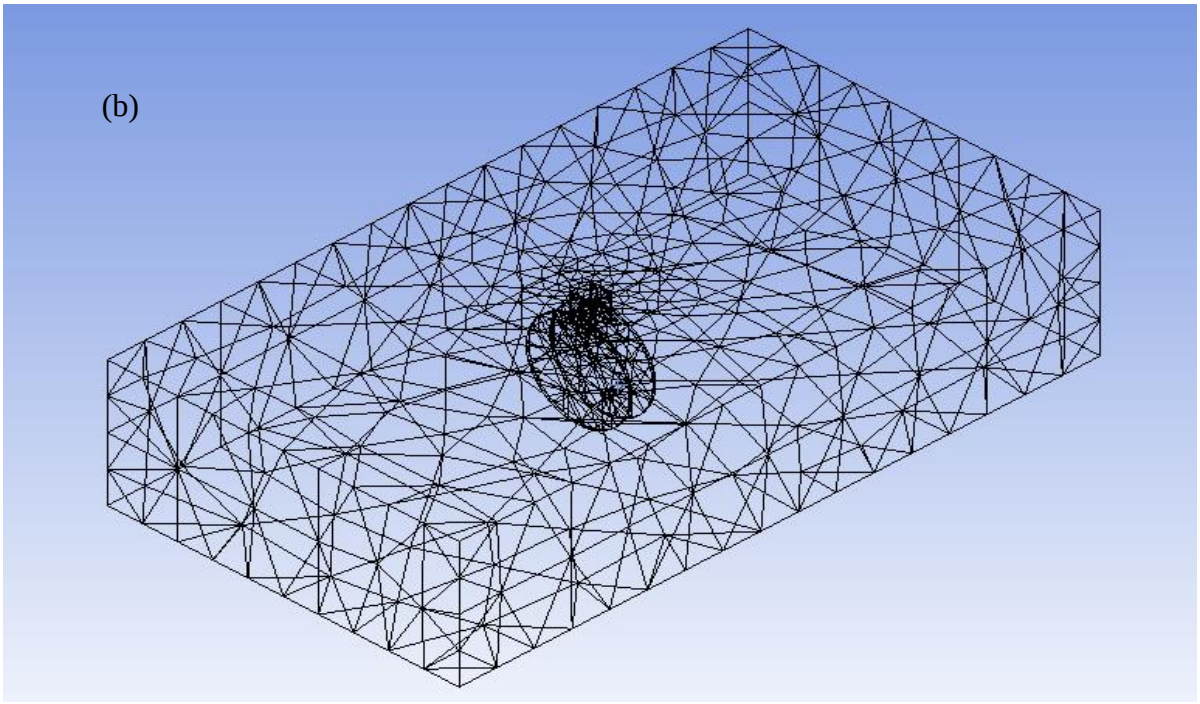

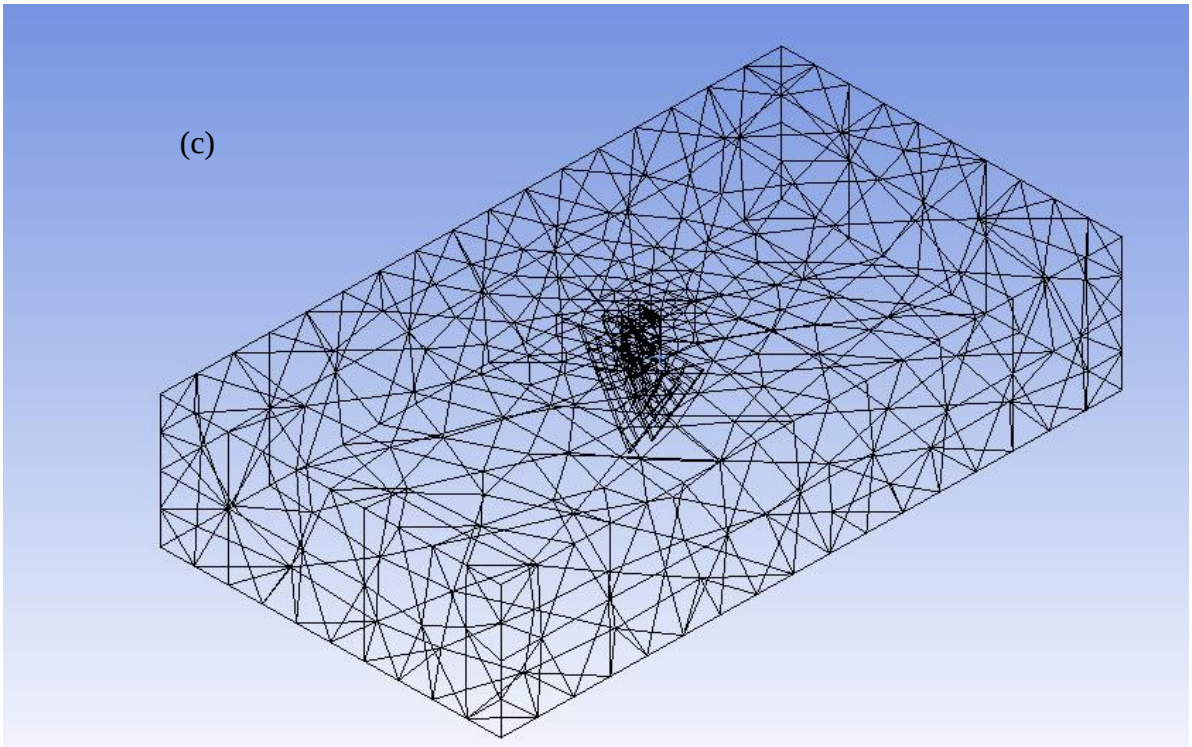

Figure 2.5 A mesh configuration for the assembly surrounded by a fluid; (a) square, (b) circular and (c) triangular PZT

2.8 Boundary Conditions

The setup for the model included applying an excitation voltage in the form of a sinusoidal wave applied to the actuator. The boundary conditions were set to restrain the plastic holder for the actuator and make the sensor holder free to move laterally to investigate the effect of distance on the wave propagation.

2.9 Harmonic Analysis and Harmonic Acoustic Analysis

The harmonic analysis included performing an analysis for the actuator under an excitation voltage in the form ($V_o \sin \omega t$); the results obtained from this analysis were transferred to the fluid medium for the next step of analysis. The results from this analysis included a deformation and voltage for the actuator.

The harmonic acoustic analysis included the fluid medium obtained from the harmonic analysis. The results in this analysis contained acoustic pressure between the actuator/sensor pair at different distances, different PZT materials and three different geometries. The frequency can be set at any range from 100 to 10 kHz.

2.10 Sensor Harmonic Analysis

This analysis included performing a second analysis to the data obtained from the harmonic acoustic analysis, which included the acoustic pressure, and applied it to the sensor. The results included the deformation and voltage for the sensor. All the detailed steps for modelling the fluid – structural interaction can be seen in appendix B.

CHAPTER 3 Results and Discussion

The acoustic harmonic analysis was made using ANSYS to investigate the acoustic wave propagations between the actuator - sensor pair surrounded by a stationary fluid. The analysis was based on the two-way *Fluid Structure Interaction* (FSI), which included an acoustic harmonic analysis to the actuator-sensor pair immersed in the fluid by solving numerically using finite element analysis through ANSYS workbench; the equation of motion for the actuator under an excitation voltage coupled with the equation of motion for the fluid domain was used to find the wave propagation in terms of acoustic pressure of the fluid between the actuator/sensor pair, deformation and voltage for both actuator and sensor pair.

The numerical solution included an investigation of three different geometries of actuator/sensor pair shown in Figure 2.2. Also, three different common piezoelectric materials were used to study the effect of their mechanical properties on the acoustic pressure waves. Finally, the effect of varying distance between the actuator/sensor pair was considered to see the effect of distance on the acoustic pressure waves pattern.

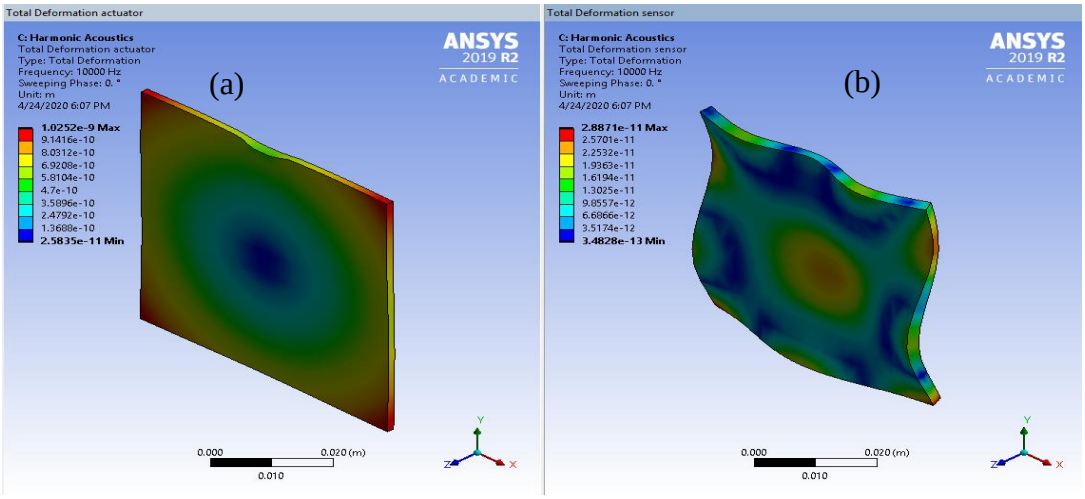

Figure 3.1 Total deformation of the actuator-sensor PZT pair for square geometry; (a) the actuator and (b) the sensor

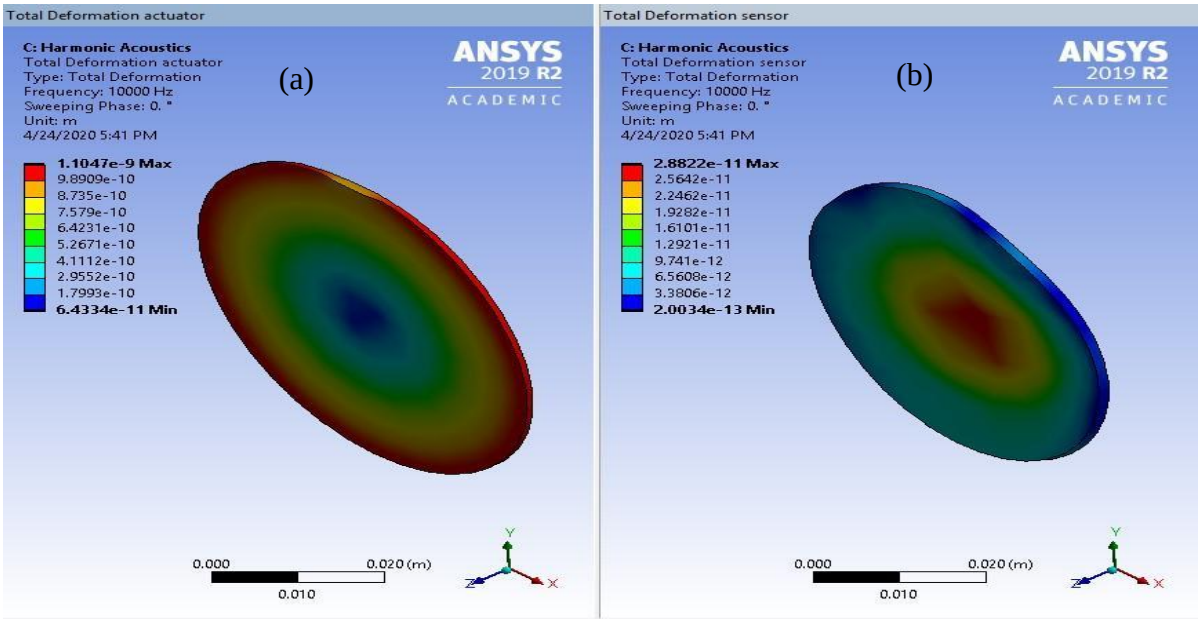

Figure 3.2 Total deformation of the actuator-sensor PZT pair for circular geometry; (a) the actuator and (b) the sensor

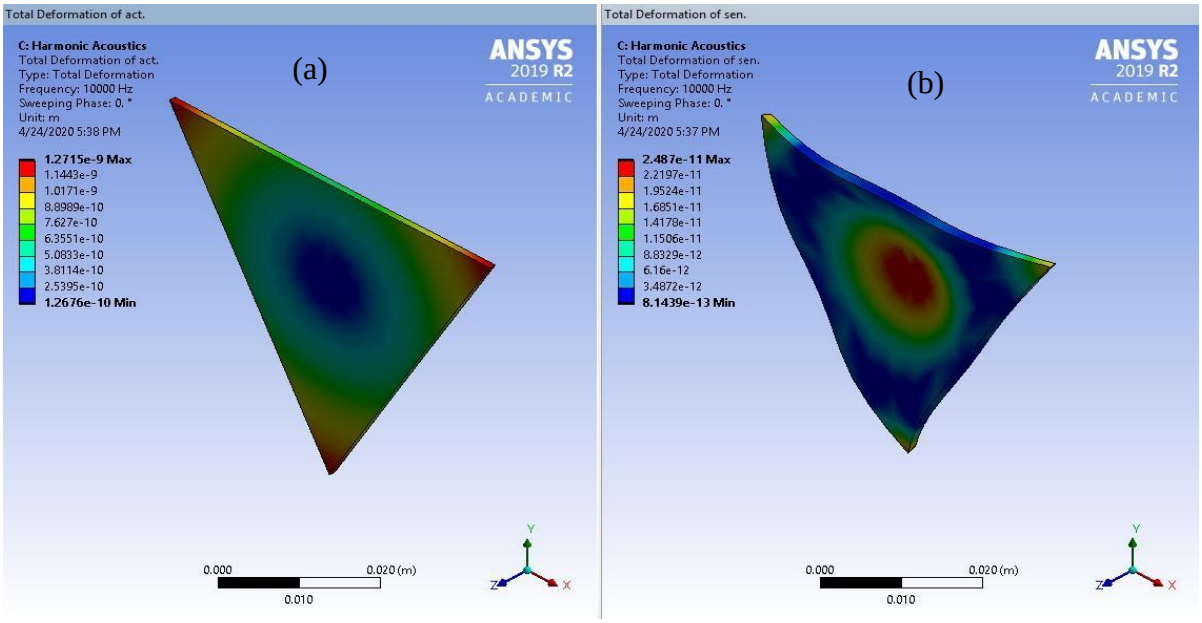

Figure 3.3 Total deformation of the actuator-sensor PZT pair for triangular geometry; (a) the actuator and (b) the sensor

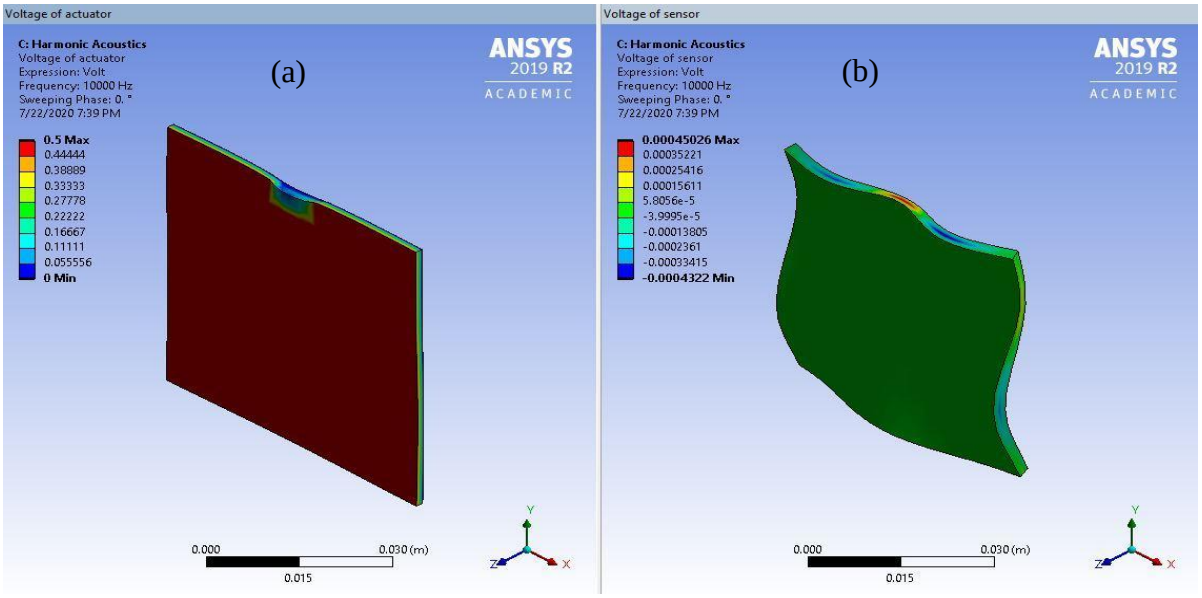

Figure 3.4 Voltage of the actuator-sensor PZT pair for square geometry; (a) the actuator and (b) the sensor

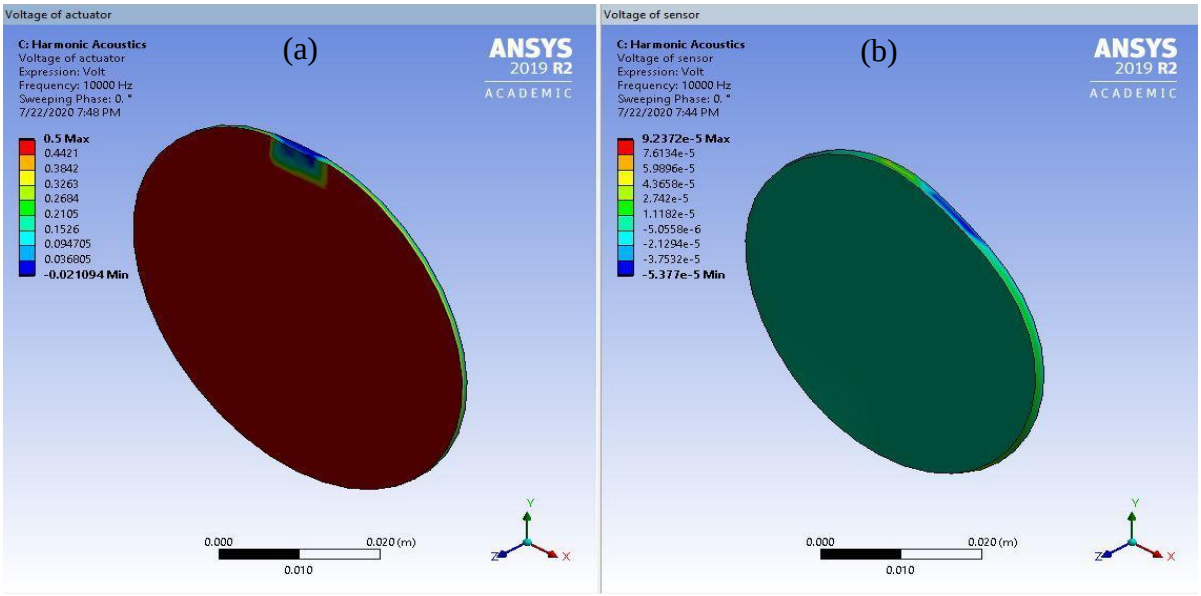

Figure 3.5 Voltage of the actuator-sensor PZT pair for circular geometry; (a) the actuator and (b) the sensor

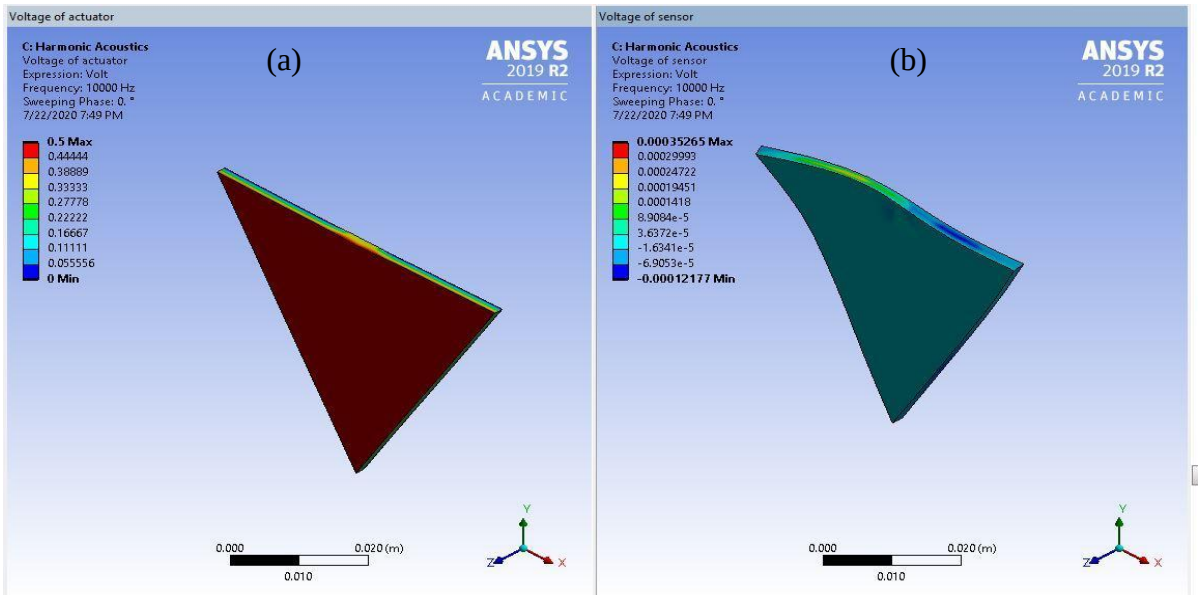

Figure 3.6 Voltage of the actuator-sensor PZT pair for triangular geometry; (a) the actuator and (b) the sensor

Figures 3.1, 3.2 and 3.3 illustrate a total deformation for the rectangular, circular and triangular actuator/sensor pair of PZT 4, respectively, when excited at 0.5 voltage and frequency of 10kHz in at distance 20 mm between the actuator/sensor pair in a solution of glycerin. From these figures, the simulations show the complexity of the deformation of the actuator and sensor with the different shapes and modes of vibration. In this case, a square actuator showed the highest deformation at the edges with several zones that do not deform at all under the generated wave. This may indicate that the perceived signal is an average at different locations. In the case of a circular and triangular shape, the highest deformation is at the center of the sensor. These two geometries may be a more suitable sensor for applications. The order of the maximum magnitude of the deformation in meters for the actuator seems to be the same for all geometries (in the order of nanometers). For the sensor however, the maximum deformations vary by magnitude and

location. In fact, the deformations perceived by the square sensor are an order of magnitude larger than the others.

Figures 3.4,3.5 and 3.6 illustrate a total voltage for the square, circular and triangular actuator sensor pair of PZT 4, respectively. It can be seen from these figures that the maximum voltage occurred on the actuator due to the voltage applied on the actuator. While the minimum values occurred on the sensor and this was due to the decay in pressure wave propagation that sensed by the sensor.

Figures 3.7, 3.8, and 3.9 demonstrate a variation of acoustic pressure with distance for square, circular and triangular PZT, respectively, at selected distances for three different PZT materials.

The maximum acoustic pressure calculated for the actuator and the sensor with varying distance is shown in Figure 3.7,3.8 and 3.9. In figure 3.7, the actuator and sensor pair are modeled with different materials and constant geometry: square PZT immersed in a solution of 100 % water, and 100% glycerin. Note that the actuator and sensor pair made with PMN32, PZT5A and PZT4. From the figures, it can be seen that the order of magnitude for the maximum acoustic pressure occurs on the PMN32, then PZT5A and PZT 4 for the same fluid, same excitation voltage and same distance. This difference in the magnitude was due to the effect of dielectric constant d_{33} for the PMN32 which is higher than PZT5A and PZT4. This leads that PMN32 is the most sensitive material to change for acoustic pressure and its slope changes more distinctively when the viscosity changes. The sensitivity in viscosity decreases when the material changes, namely PZT 5A (soft) and last PZT4 (hard) being the least sensitive. More results of the acoustic pressure variations with different distances can be seen in Appendix (C).

Also, the acoustic pressure for both the sensor and the actuator with varying distance for different geometries and for PZT pair made of PMN32 immersed in a solution of 100% water and 100% glycerin are shown in Figures 3.10,3.11 and 3.12. The geometry of the sensor/actuator pair was made of PMN32, PZT5A and PZT 4, respectively, and different geometries. It can be seen that maximum acoustic pressure occurred when the square geometry with PMN32 was used. These changes in acoustic pressure were due to the surface area for the square being larger than the circle and triangle geometries. All other results of acoustic pressure variation with other distances, geometries and PZT materials can be seen in appendix D.

In addition, it can be seen that for the same boundary conditions, the acoustic pressure was mainly influenced by fluid density and speed of sound. This effect can be clearly seen given the order of magnitude between the acoustic pressure for glycerin versus water.

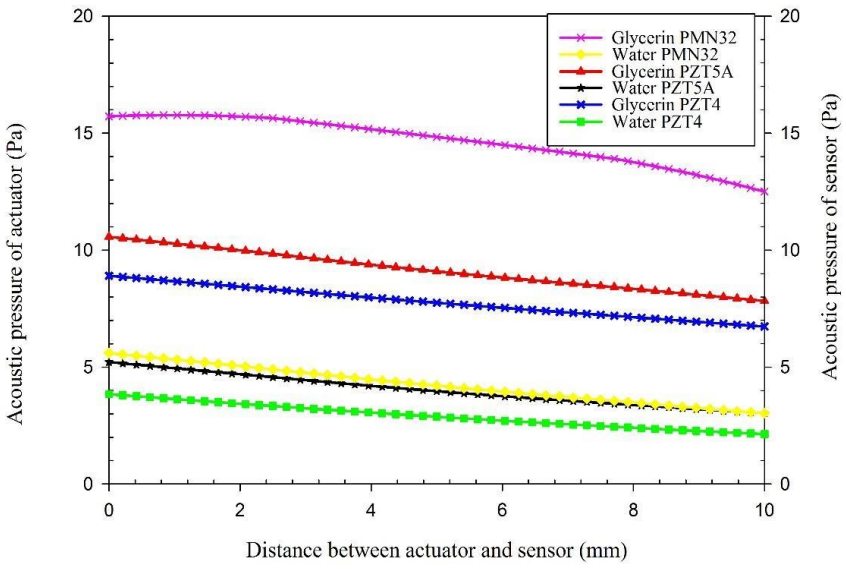

Figure 3.7 Acoustic pressure variations vs distance (10mm) for square actuator/sensor PZT pair made of PMN32, PZT4, and PZT5A; immersed in 100 % glycerin and 100 % water

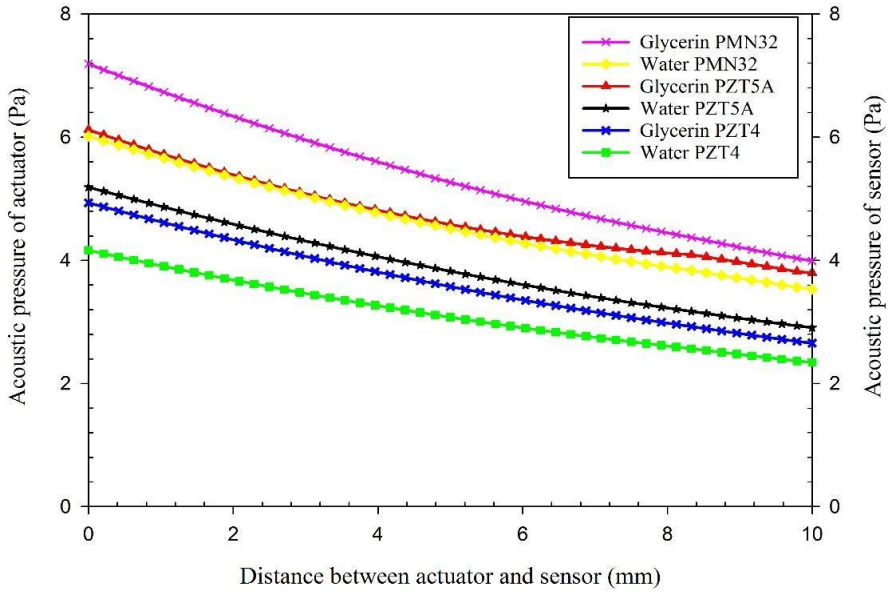

Figure 3. 8 Acoustic pressure variations vs distance (10mm) for circular actuator/sensor PZT pair made of PMN32, PZT4, and PZT5A; immersed in 100 % glycerin and 100 % water

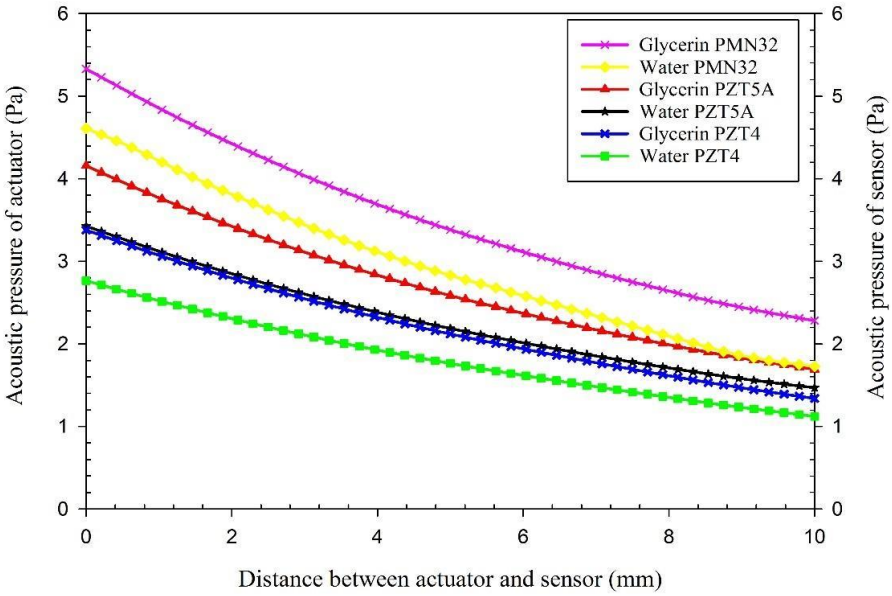

Figure 3.9 Acoustic pressure variations vs distance (10mm) for triangular actuator/sensor PZT pair made of PMN32, PZT4, and PZT5A; immersed in 100 % glycerin and 100 % water

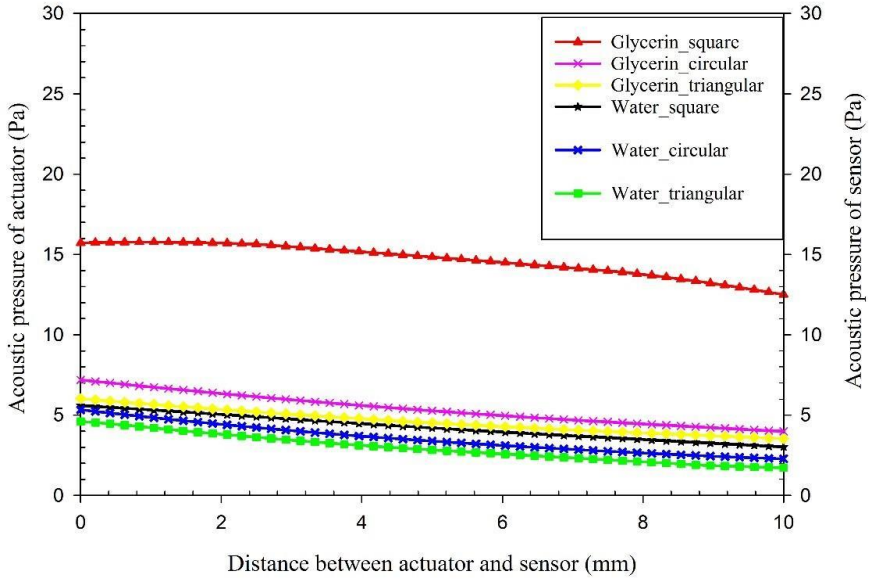

Figure 3.10 Acoustic pressure variations vs distance (10mm) for actuator/sensor PZT pair for different geometries made of PMN32; immersed in 100 % glycerin and 100 % water

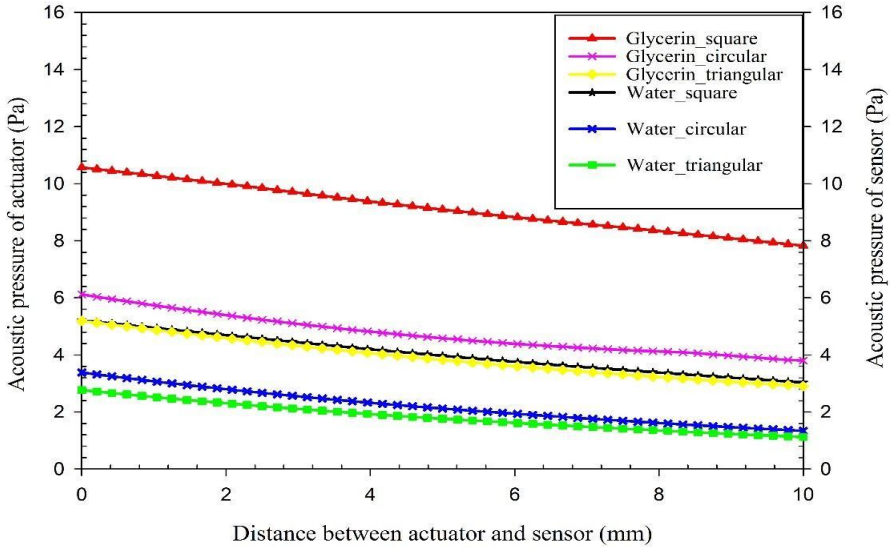

Figure 3.11 Acoustic pressure variations vs distance (10mm) for actuator/sensor PZT pair for different geometries made of PZT5A; immersed in 100 % glycerin and 100 % water

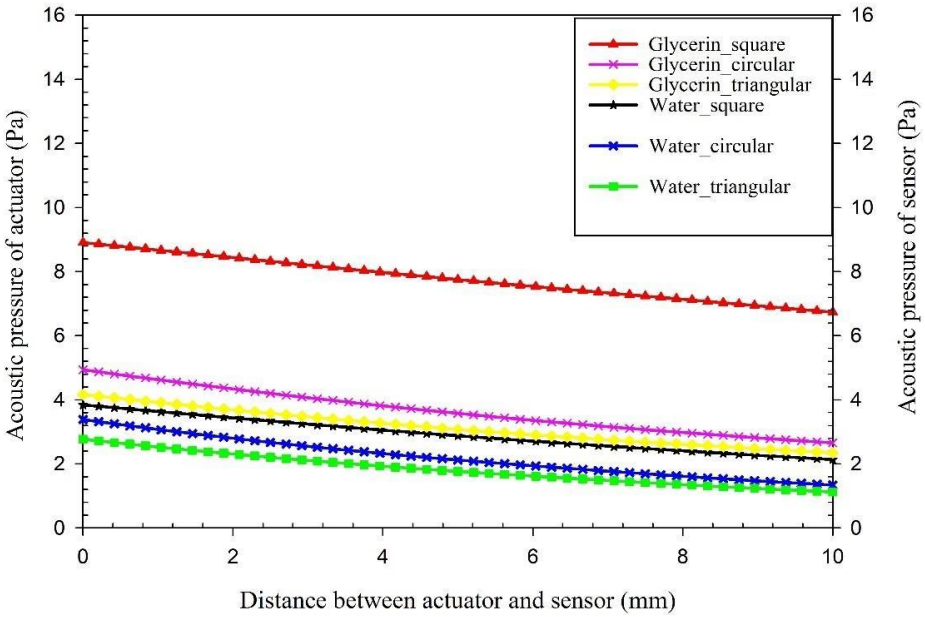

Figure 3.12 Acoustic pressure variations vs distance (10mm) for actuator/sensor PZT pair for different geometries made of PZT4; immersed in glycerin and water

Also, the numerical simulation studied the effect of mesh quality on the simulation. This study included using three different mesh qualities (Coarse, medium and fine mesh) for both solid structure (actuator/sensor pair) and fluid domain (water and glycerin) to see their effect on the results, especially the acoustic pressure. Tables 3.1, 3.2 and 3.3 shows the effect of mesh quality on the acoustic pressure. It can be seen that from the tables that there is no significant effect of mesh quality on the acoustic pressure with different geometries, PZT materials and fluid type.

Table 3.1 Effect of Mesh Quality using Square Shape, varying Piezoelectric Material type, and Fluid, on the Acoustic Pressure

Mesh Quality	Geometry	No. of Nodes	No. of Elements	Material	Fluid	Max Acoustic Pressure (Pa)	Min. Acoustic Pressure (Pa)
Coarse		12807	7730	PMN32	Glycerin	29.0	20.9
Medium	Square	13586	8190	=	=	29.2	21.1
Fine		15170	9147	=	=	29.4	21.2
Coarse		12807	7730	PMN32	Water	9. 5	3.1
Medium	Square	13586	8190	=	=	9.5	3.1
Fine		15170	9147	=	=	9.5	3.1
Coarse		12807	7730	PZT 5A	Glycerin	18.8	13.4
Medium	Square	13586	8190	=	=	18.8	13.3
Fine		15170	9147	=	=	18.9	13.4
Coarse		12807	7730	PZT 5A	Water	6.8	2.3
Medium	Square	13586	8190	=	=	6.8	2.4
Fine		15170	9147	=	=	6.8	2.4
Coarse		12807	7730	PZT 4	Glycerin	10.4	7.0
Medium	Square	13586	8190	=	=	10.4	7.1
Fine		15170	9147	=	=	10.4	7.1
Coarse		12807	7730	PZT 4	Water	4.1	1.5
Medium	Square	13586	8190	=	=	4.1	1.5
Fine		15170	9147	=	=	4.1	1.5

Table 3.2 Effect of Mesh Quality using Triangular Shape, Piezoelectric varying Material Type and Fluid, on the Acoustic Pressure

Mesh Quality	Geometry	No. of Nodes	No. of Elements	Material	Fluid	Max. Acoustic Pressure (Pa)	Min. Acoustic Pressure (Pa)
Coarse		3465	3341	PMN32	Glycerin	19.0	5.1
Medium	Triangular	4723	3341	=	=	19.0	5.1
Fine		5653	3341	=	=	19.0	5.1
Coarse		3465	3341	PMN32	Water	15.5	4.2
Medium	Triangular	4723	3341	=	=	15.5	4.3
Fine		5653	3341	=	=	15.5	4.3
Coarse		3465	3341	PZT 5A	Glycerin	5.0	1.3
Medium	Triangular	4723	3341	=	=	5.0	1.3
Fine		5653	3341	=	=	5.0	1.3
Coarse		3465	3341	PZT 5A	Water	4.1	1.1
Medium	Triangular	4723	3341	=	=	4.1	1.1
Fine		5653	3341	=	=	4.1	1.1
Coarse		3465	3341	PZT 4	Glycerin	3.8	1.0
Medium	Triangular	4723	3341	=	=	3.8	1.0
Fine		5653	3341	=	=	3.8	1.0
Coarse		3465	7730	PZT 4	Water	3.1	0.8
Medium	Triangular	4723	8190	=	=	3.1	0.8
Fine		5653	9147	=	=	3.1	0.8

Table 3.3 Effect of Mesh quality using Circular Shape, varying Piezoelectric Material Type, and Fluid on the Acoustic Pressure

Mesh Quality	Geometry	No. of Nodes	No. of Elements	Material	Fluid	Max. Acoustic Pressure (Pa)	Min. Acoustic Pressure (Pa)
Coarse		5544	3439	PMN32	Glycerin	27.5	11.0
Medium	Circular	5653	3439	=	=	27.5	11.0
Fine		8407	5560	=	=	27.8	11.1
Coarse		5544	3181	PMN32	Water	22.6	9.8
Medium	Circular	5653	3439	=	=	22.6	9.8
Fine		8407	5560	=	=	23.1	9.7
Coarse		5544	3181	PZT 5A	Glycerin	7.2	2.3
Medium	Circular	5653	3439	=	=	7.2	2.3
Fine		8407	5560	=	=	7.2	2.8
Coarse		5544	3181	PZT 5A	Water	6.1	2.5
Medium	Circular	5653	3439	=	=	6.1	2.5
Fine		8407	5560	=	=	6.0	2.5
Coarse		5544	3181	PZT 4	Glycerin	5.5	2.1
Medium	Circular	5653	3439	=	=	5.5	2.1
Fine		8407	5560	=	=	5.4	2.1
Coarse		5544	3181	PZT 4	Water	4.6	1.9
Medium	Circular	5653	3439	=	=	4.6	1.9
Fine		8407	5560	=	=	4.6	1.9

In order to validate the simulation, a simple experiment described in Chapter 2 was performed. In this case, two simple experiments were done using two circular PZT immersed into 100% water and 100 % glycerin. A voltage signal of 0.5 V was applied to the actuator in the form of sinusoidal wave with frequency range from 100 Hz to 40 MHz using impedance analyzer.

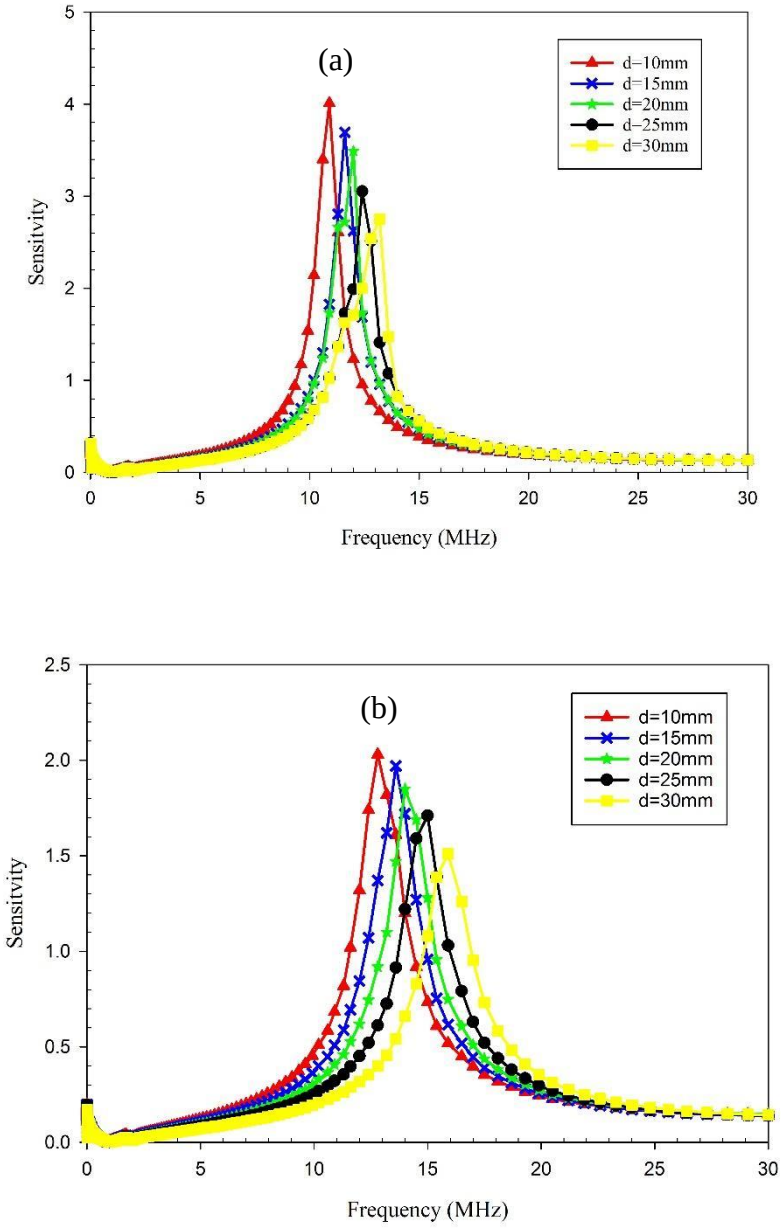

Figure 3.13 Experimental measurements of gain vs. frequency at different distances between the circular PZT5A actuator and sensors immersed in (a) glycerin and (b) water

The validation between the numerical and experimental results included a calculation of the pressure sensitivity which represents the ratio of the $P_{sen.}/ P_{act..}$ from the numerical simulation for the circular PZT pair at a certain distance. The experimental calculation included pick up values for gain for the circular PZT at the same distance as in the numerical simulation at frequency of 10 kHz. Then, the sensitivity db value was calculated for both numerical and experimental results using the equations (3.1) and (3.2):

$$db_{num.} = 20 \left| log \ \frac{P_{sen}}{P_{act}} \right| \tag{3.1}$$

$$db_{exp.} = 20|log \ \ sensitvity \ | \tag{3.2}$$

From equations 3.1 and 3.2 the values of sensitivity db for both numerical and experimental results were calculated. The values show that the numerical sensitivity ($db_{num.}$) were 10.825 and 11.4 for water and glycerin, respectively, while, the values of the experimental sensitivity ($db_{exp.}$) were 11.254 and 18.48 for water and glycerin, respectively. From those values it can be seen that there's small difference between the numerical and experimental values for the water. However, this difference is bigger in the case of the glycerin; this is because of the inaccuracy of the reading for the measuring values.

Also, Figures 3.14 and 3.15 show the variation of numerical acoustic pressure sensitivity and experimental voltage sensitivity with the distance between the actuator /sensor pair for glycerin and water, respectively.

From both figures, it can be seen that there was an exponential decay for numerical and experimental results in both fluids. This decay was mainly affected by several

factors such a distance between the actuator/sensor pair, frequency, fluid viscosity, fluid density and speed of sound into the different fluid media.

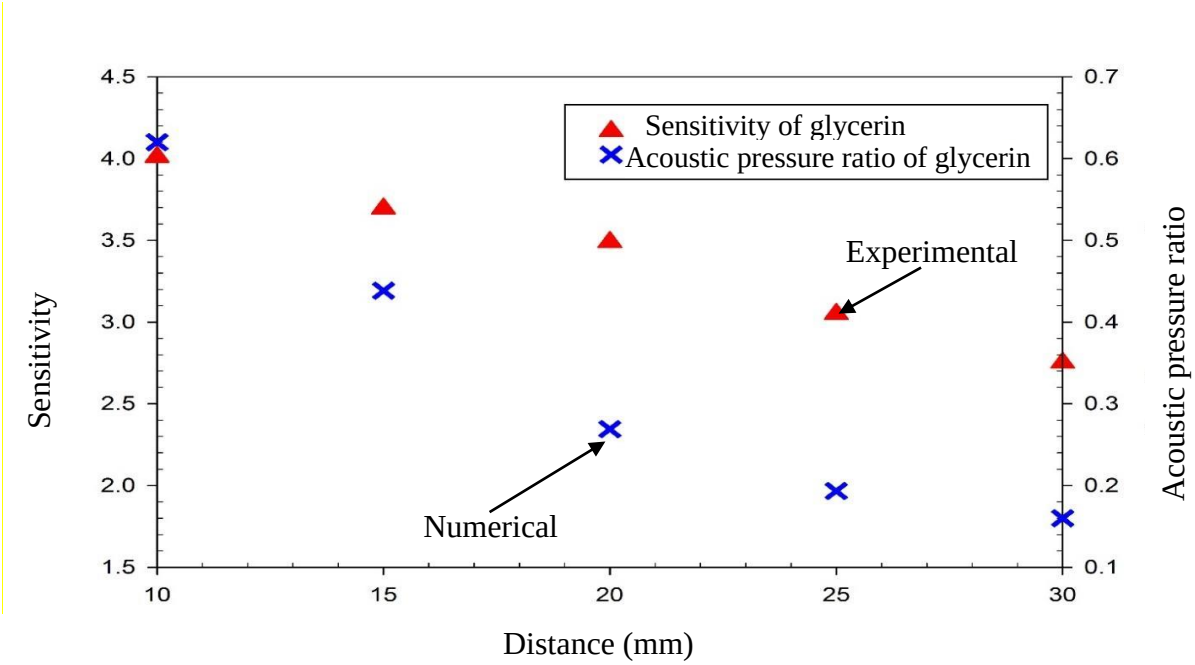

Figure 3.14 Variation of distance with sensitivity and acoustic pressure for glycerin

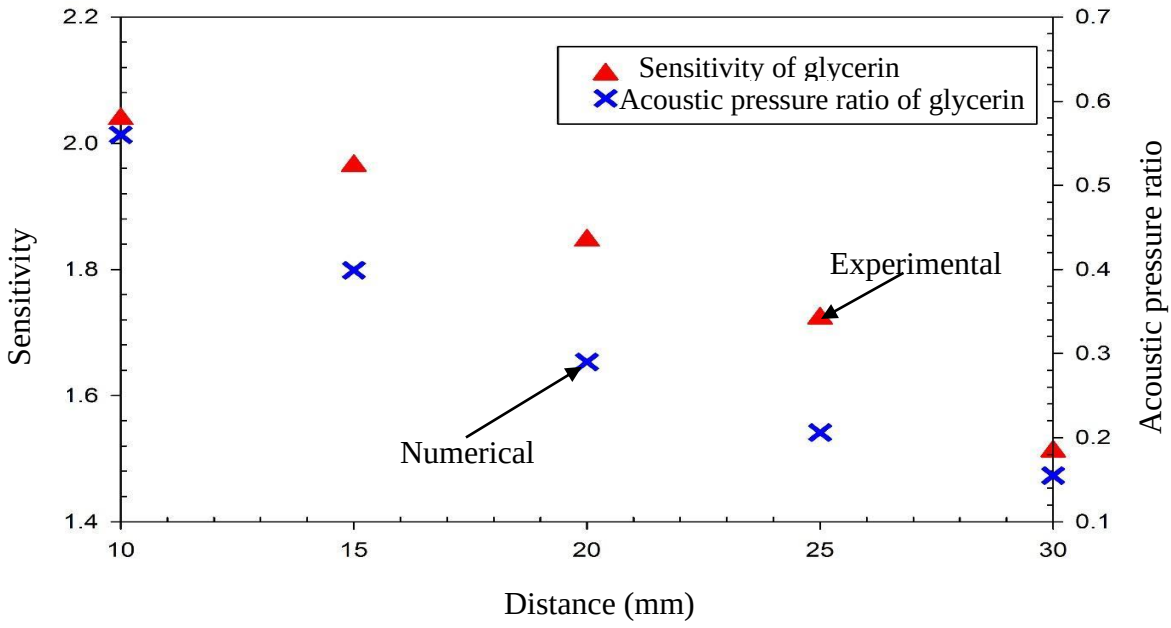

Figure 3.16 Variation of distance with sensitivity and acoustic pressure for water

CHAPTER 4 Non-destructive evaluation viscosity device

Monitoring of fluid viscosity is very important in many different industries ranging from oil industry to healthcare applications [85-88]. For example, in the oil and petroleum industry, viscosity measurements play a vital role in determining the oil quality and how it can affect the pipeline [89]. In the healthcare industry, monitoring blood viscosity is crucial for the treatment of some diseases, such as vascular-related diseases [90]. Standard laboratory such as viscometers, capillary tubes and rotating devices, need long measurement times and a large volume sample [91]. In addition, these devices can be expensive and require specialized training [91, 92], and they are unable to measure viscosity in real - time continuously. Therefore, there is an increasing need for accurate, real time, and low – cost viscosity measurement devices. Hence, a wide variety have been developed over the years to establish high sensitivity, small size, ease of manufacture and use, real-time measurement, and low-cost [90-95]. Modern viscosity measurement devices can be categorized based on their operational principle of monitoring parameters such as (a) displacement, (b) vibrations, and (c) wave propagation in fluids of different viscosities [87, 96, 57]

The displacement device basically works by correlating the viscosity of fluid to the displacement of a ferromagnetic piston between two electromagnetic coils [97]. Also, there is a recent method for viscosity measurement sensors based on measuring the amplitude and phase responses to displacement of the sensor in the fluid using a fiber -optic method [94]. Zhang et al [98] demonstrated a system that utilizes a Pb (Zn(1/3)Nb(2/3))O(3−x)PbTiO(3) (PZN-PT) cantilever probe for actuation and a laser displacement sensor for detection. Though these devices are designed for specific applications, they usually work within a constrained low range of viscosity values and require specialized equipment such as optic fibers and lasers.

Regarding vibration-based devices, a wide variety are available. One typical example consists of a piezoelectric cantilever sensor, which correlates the resonance frequency shift and fluid viscosity [99,100]. Similarly, measuring the resonance frequency of a vibrating beam by applying a Lorentz force generated by an Alternating Current (AC) in a permanent magnetic field is another mechanism that has been explored [101,102].

Similarly, quartz thickness-shear mode sensors are adapted to measure viscosity [90]. This type of sensor, in particular, monitors the process of platelet activation, which leads to thrombus formation (clotting). By following the sensors admittance frequency shifts concerning different concentrations of platelet activation, coagulation can be detected. Purohit et al [103] reported a radial mode piezo-resonator disc to improve the ultrasonic determination of viscosity in liquids by correlating resonant frequency changes to viscosity. Another type of quartz thickness-shear mode sensor is worth mentioning is a capacitive micromachined transducer [95, 104], which utilizes a non-destructive ultrasonic pulse-echo system using piezoelectric materials as membrane sensors and actuators. The changes to the waveform received due to mass changes correlate to viscosity. With the development of microelectromechanical systems (MEMS) technology, viscosity, and density measurements of different fluids are possible [88, 93, 105-109]. However, issues, including inaccurate estimation, low range of viscosities, lack of analytical models, and complex calibration procedures, remain barriers with these types of devices [93, 105, 107, 110].

Wave propagation-based devices use the measurement of the propagation time of wave in a fluid and correlate the result to the fluid viscosity. For instance, a piezoelectric sensor sends a signal to a liquid medium, and a reflector sends the signal back to the device [111]. The reflected wave impedance is then measured and correlated to viscosity. This method requires a reflector and

a large container and sample volume. This method has been widely used in structural health monitoring of solids or structures for years.

In this chapter, a new device for monitoring a viscosity using non-destructive evaluation method was designed and built. The purpose of the device is to demonstrate non-destructive evaluation techniques in fluids to detect viscosity changes. In this application, the device must be small enough to fit into a 3 ml vacutainer for use within the healthcare industry.

4.1 Design

In this section a design of viscosity probe device was proposed as an application of non-destructive evaluation technique. The design consists of a piezoelectric sensor and actuator device pair based on a tuning fork principle using an actuator/sensor pair. The device design constraints were size (small footprint, portability) and marketability (ease of manufacture, low cost, and expendable). A commercially available soft PZT (type 5A) was chosen for the sensor and actuator pair to satisfy marketability requirements. The PZT is bonded to a hollow brass tube, which is used to accommodate wiring on two opposite sides allowing the device to share a ground connection. The piezoelectric material that serves as an actuator vibrates as a function of the applied voltage signal, $V_o \cdot sin(\omega t+\phi_o)$ where V_o is the applied voltage at a particular frequency ($f = \omega/2\pi$) and an initial phase angle $\phi_o = 0$. The actuator produces sound pressure waves that travel approximately 5 mm through the fluid medium to the sensor that then records a waveform with an amplitude, V_r or received voltage, and a phase angle ϕ_r, $V_R \, sin(wt+\phi_r)$. The proposed method is illustrated in Figure 4.1.

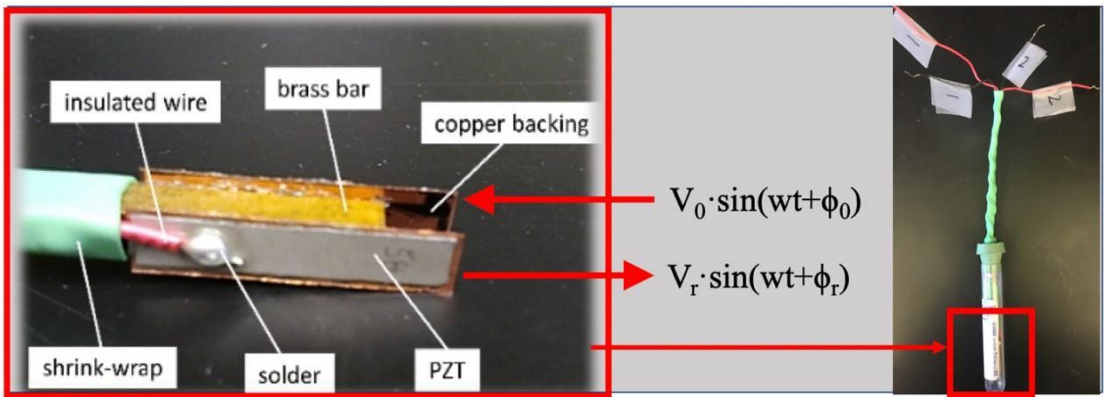

Figure 4.1 Probe construction and operation

4.2 Fabrication

4.2.1 Materials

After considering several prototypes, the device was built consisting of layered materials bonded with a conventional adhesive at room temperature. The layers help to ensure structural integrity and ruggedness. These layers consisted of (a) two rectangular plates of PZT polarized with Nickel electrodes (23 x 5 mm with thickness of 1 mm by Morgan Matroc Ceramics); (b) two copper layers (25 x 6 mm with thickness of 1 mm); and (c) a rectangular hollow bar with a square cross-section made of brass (70 x 5 mm with thickness of 5 mm). The layers can be shown in Figure 4.1.

4.4.2 Assembly

The assembly consisted of a square hollow brass bar coated with polyethylene to provide electrical insulation. Then, two thin layers of Copper (0.1 cm) and PZT (0.1 cm) were placed with an adhesive to two of the outside opposing faces of the bar. Wires were soldered to the PZT surfaces for a positive connection, and the copper layer becomes the ground. Heat shrink-wrap was used to secure the cables in place and minimize the footprint of the device. The final prototype

fits easily inside a standard vacutainer (Lithium Heparin 56USP with a diameter of 13 mm, a capacity of 3 mL, and tube length of 75 mm).

4.3 Experimental Setup

Once the prototype is completed, a method that provides a consistent volume ratio of the several mixtures of glycerin and water was required. For experimental testing, the volume was kept constant at approximately 0.75 mm^3 measured using a syringe. In this manner, only the tip of the probe was submerged in the liquid.

LabView® software records and controls a Hewlett Packard 4194A Impedance/Gain-Phase Analyzer capable of measuring capacitance, impedance, gain, and phase angles. The analyzer scanned frequencies and supplied a sinusoidal wave to the actuator and monitored the signal received by the sensor. The applied signal was a sinusoidal wave with an amplitude of 0.5 Volt at a range of frequencies between 100 Hz and 40 MHz. The measured gain and phase are the ratio of the amplitudes and the phase difference between the two signals. All measurements were performed in a custom-made Faraday cage to avoid interference in the high-frequency ranges. Figure 4.2 illustrates the experimental setup of the viscosity probe.

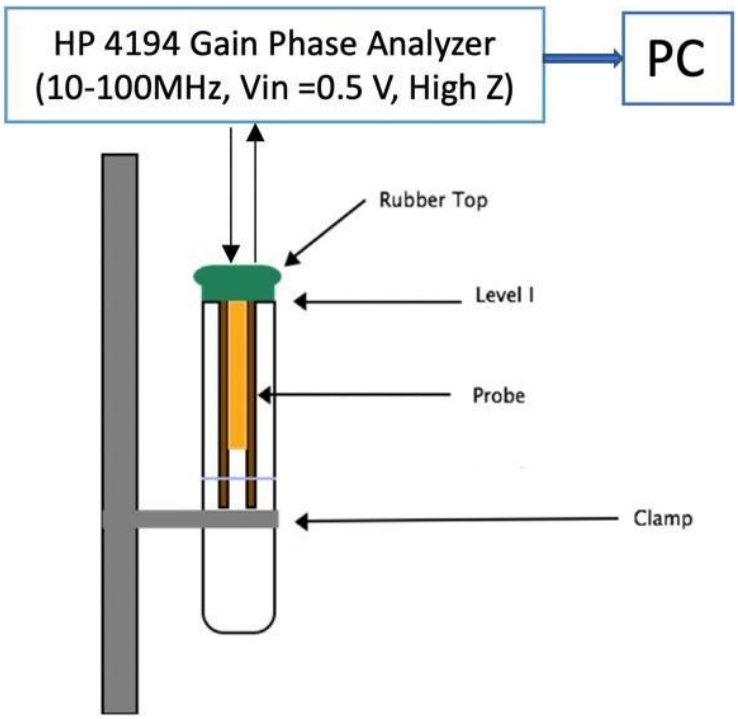

Figure 4.2 Experimental setup of the viscosity probe

In addition to the Gain-Phase measurements, the impedance of the device in different liquids was also monitored. The range of frequencies was smaller since piezoelectric devices consume more current at the higher frequencies, and the impedance is not measured accurately at higher values. The following steps summarize procedures of a typical set of experiments: Measuring (1) the impedance of the actuator or sensor in water and glycerin; and; (2) the gain-phase with two different concentrations and mixtures of distilled water (DI) and glycerin.

4.4 Experimental Results

The experimental results include measuring and recording phase shifts of the frequency in glycerin and DI-water (Deionized water) mixture of various concentrations are plotted for the probe, as shown in Figure 4.3. The phase shift is defined as the difference between the phase angle

of the sent signal and the received one. The frequency of the applied signal was scanned for the entire range the Gain-Phase analyzer is capable of performing (100Hz to 40MHz).

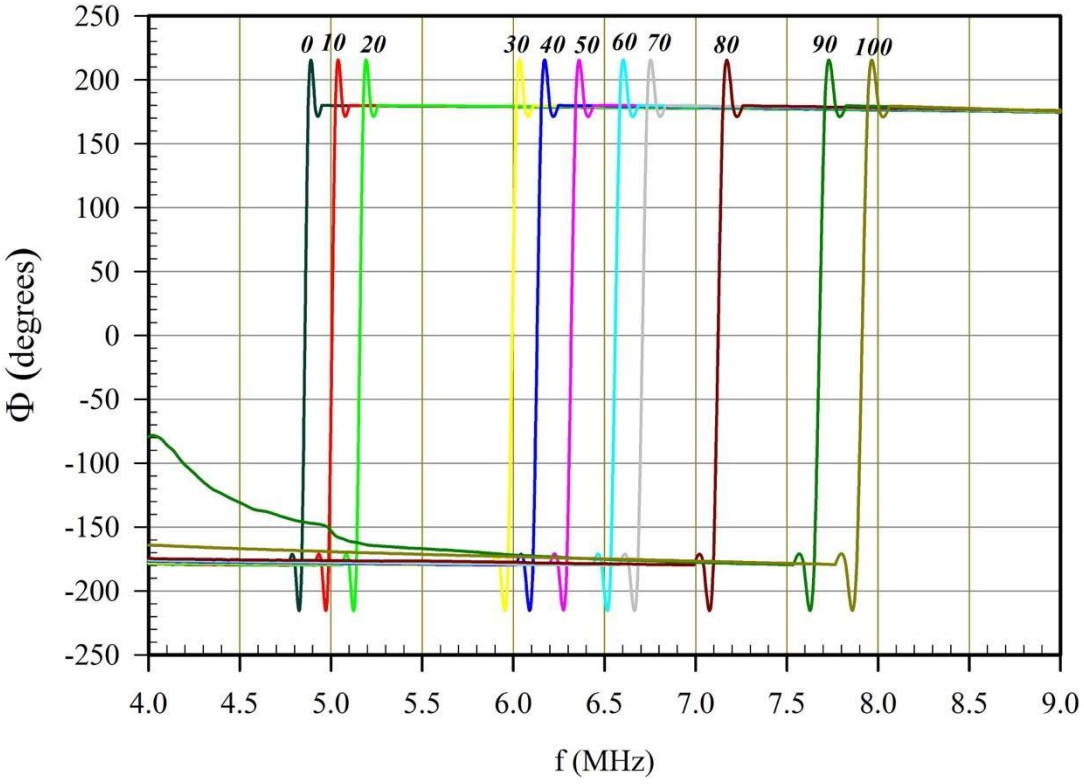

Figure 4.3 Peak phase shift vs. frequency as detected by the Gain-Phase Analyzer at different Glycerin concentrations (0 to 100%)

Since the probe is a prototype, there is room for some variability. Thus, quality assurance tests were crucial in determining prototype integrity. One way to monitor this integrity was periodically monitoring capacitance and impedance values, since changes on the measured values may indicate delamination, cracks, or deficiencies in the probe. Phase shifts for each glycerin level were compared to known respective viscosity values, in the form of a calibration curve. Known glycerin viscosities regarding both temperature and solution percentage can be obtained from available literature [112]. A detailed error and p-values of the regression, as well as the values of the

coefficient, are shown in Table 4.1. A statistical analysis of the regression was performed, with the R^2 of 0.99, indicating that the data fits a profile of the form is defined as follows.

$$\nu = ae^{-\frac{1}{2}\left(\frac{f_R - f_0}{b}\right)^2}, \tag{4.1}$$

where ν is the viscosity in cP, f_R is the resonance frequency (MHz), f_0, and a, and b are constants that could be related to damping and sound propagation. Though the R^2 was high, the parameters may not be quite accurate (coefficients have a high standard error and high p-values). This type of equation is usually used for a Gaussian wave equation and maybe significant in calibrating and predicting viscosity values. The large standard errors indicate multi-colinearity, which indicates more refinement of this equation is needed and more data is required for a more definite model. The purpose of Equation (4.1) is to illustrate the trends observed in the experiments.

Table 4.1 Statistical analysis of the regression

R	R^2	Adjusted R^2	Standard Error of Estimate	
0.9987	0.9975	0.9969	22.19	
	Coefficient	Std. Error	t	P
a	1341.292	342891640	3.91E-006	1.00
b	0.115	118380	9.73E-007	1.00
f_0	7.365	213305	3.687E-005	1.00
Analysis of Variance				
		DF	SS	MS
Regression		3	1812696	604232
Residual		8	3940	492

The results of the regression and confidence intervals are shown in Figure 4.4 that illustrates the viscosity variation of different glycerin/DI water concentration levels with the frequency shifts. It can be seen from the graph that the frequency shift increases with increases of viscosity (increases in glycerin concentration).

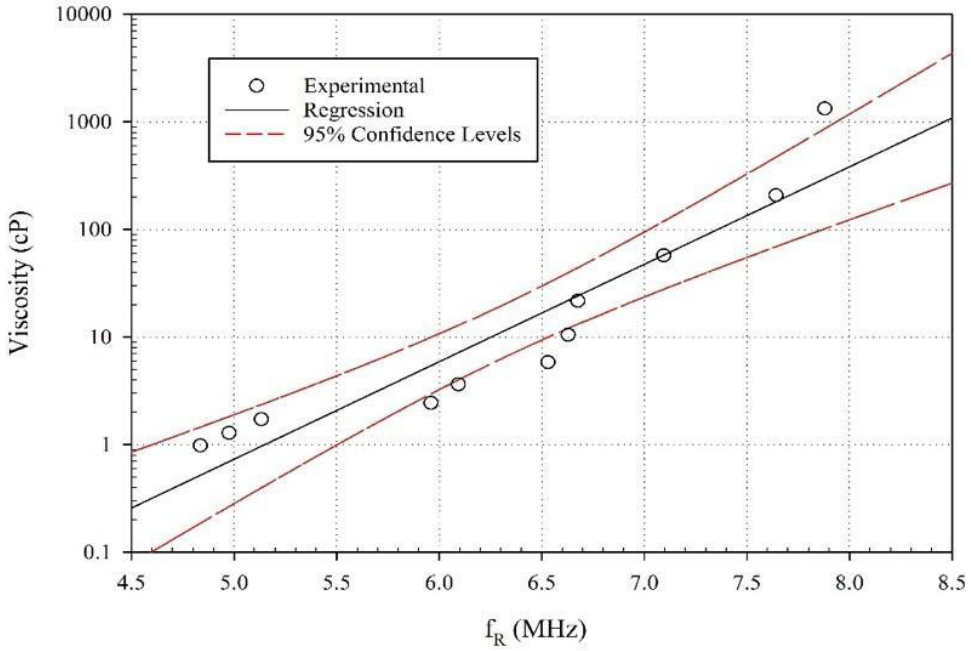

Figure 4.4 Frequency vs viscosity regression

All the cases tested experimentally were also modeled, and the results are shown in Figure 4.3. In spite of these differences, the trend is clear: higher viscosity results in a higher frequency shift.

4.5 Modeling of Non-Destructive Evaluation Device

The modeling of the non-destructive evaluation device included creating a computer model of the piezoelectric viscosity probe built with dimensions of 5 x 5 x 70 mm, two copper sheets

with dimensions of 6 x 0.1 x 25 mm, and two pieces of PZT type 5A with dimensions of 5 x 0.1 x 23 mm. Figures 4.5a, b and c show a diagram of the device assembly created using SolidWorks®.

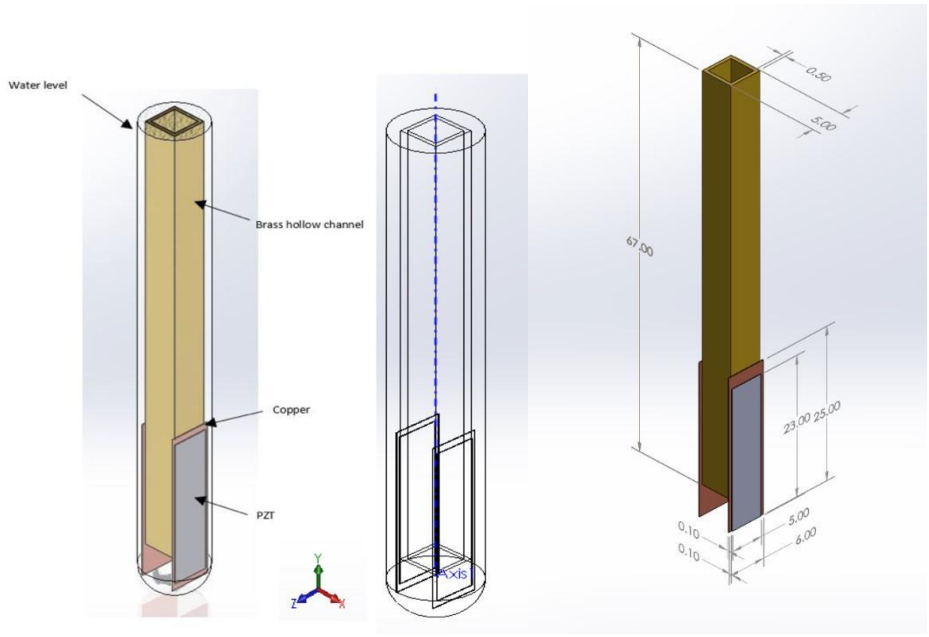

Figure 4.5 Model built in SolidWorks®: (a) schematic of the built model and fluid level; (b) the layers of the model; and (c) Prototype dimensions in mm

4.5.1 Material Properties

Mechanical properties for all materials are listed in Table 4.2. All materials utilized in the probe were assumed to be isotropic except for the PZT material [82].

Table 4.2 Mechanical properties for the viscosity probe

Material	Piece #	Dimensions (mm)	Density (kg/m^3)	Modulus of Elasticity (N/m^2)
Hollow brass	1	5 x 5 x 70	8500	96E+9
Copper	2	6 x 0.1 x 25	8900	110E+9
PZT 5A	2	5 x 0.1 x 23	7550	Appendix(A)

The piezoelectric material properties [83] for the PZT- 5A are defined as:

$$\left[\frac{\varepsilon}{\varepsilon_0}\right] = \begin{bmatrix} K_{11} & 0 & 0 \\ 0 & K_{11} & 0 \\ 0 & 0 & K_{33} \end{bmatrix} \quad (4.1)$$

$$[e] = \begin{bmatrix} 0 & 0 & e_{31} \\ 0 & 0 & e_{31} \\ 0 & 0 & e_{33} \\ 0 & 0 & 0 \\ 0 & e_{15} & 0 \\ e_{15} & 0 & 0 \end{bmatrix} \quad (4.2)$$

$$[\mathrm{C}] = \begin{pmatrix} C_{11} & 0 & 0 & 0 & 0 & 0 \\ C_{21} & C_{22} & 0 & 0 & 0 & 0 \\ C_{31} & C_{32} & C_{33} & 0 & 0 & 0 \\ C_{41} & C_{42} & C_{43} & C_{44} & 0 & 0 \\ C_{51} & C_{52} & C_{53} & C_{54} & C_{55} & 0 \\ C_{61} & C_{62} & C_{63} & C_{64} & C_{65} & C_{66} \end{pmatrix} \quad (4.3)$$

where $[\varepsilon/\varepsilon_0]$ is the relative permittivity, [e] is the coupling (in C/m^2), and [C] is the elasticity matrices in (Pa), respectively.

4.5.2 Meshing

The mesh configuration for the viscosity probe and the surrounded fluid is assumed to be the same mesh configuration mentioned in section 2.7. Figure 4.6 shows a mesh configuration for the PZT assembly surrounded by a fluid domain.

Figure 4.6 A mesh configuration for the viscosity probe surrounded by a fluid domain

4.5.3 Setup

The setup for the model included applying an excitation voltage in the form of sinusoidal wave applied to the actuator. Also, boundary conditions were applied which included restraining the top of the probe to be consistent with the experiments to $u = u_x = u_y = u_z = 0$.

4.6 Solver

Once the setup was done, the solver in the ANSYS Workbench was used to the run the model and do the analysis.

4.6.1 Modal Acoustic Analysis

The modal acoustic analysis with ANSYS was used to calculate the mode shapes of vibration for the probe and the surrounding fluid. In this manner, the natural resonant and vibration modes can be ruled out as a factor in the observed viscosity changes with frequency.

4.6.2 Harmonic Acoustic Analysis

This analysis used a two-way Fluid Structure Interaction (FSI) to find the phase shift actuator/sensor PZT pair under the excitation of the applied voltage.

4.7 Numerical Results

In this case, a model acoustic analysis with ANSYS was used to calculate the mode shapes of vibration for the probe and the surrounding fluid domain. In this manner, the natural resonant and vibration modes can be ruled out as a factor in the observed viscosity changes with frequency. The natural frequencies for the probe immersed into air, water and glycerin solution are listed in Table 4.3.

Table 4.3 Natural frequency for the probe of different fluids in (Hz)

Fluid	Density (kg/m^3)	Speed of sound (m/s)	Mode 1	Mode 2	Mode 3
Air	1.2	343	683.86	684.24	2358
Water	1000	1484	499.88	533.88	1080.2
Glycerin	1260	1920	468.53	501.72	625.45

Also, by using ANSYS, numerical simulations and analysis was performed. This analysis used a two-way FSI to find the phase shift actuator/sensor PZT pair under the excitation of the applied voltage. Figure 4.7 illustrates the phase shift change for the simulated and experimental for both distilled water and glycerin, respectively. Also, Figure 4.8 shows the variation of resonant frequency with viscosity of the fluid for both numerical and experimental work, and demonstrates the close agreement between the numerical and experimental results.

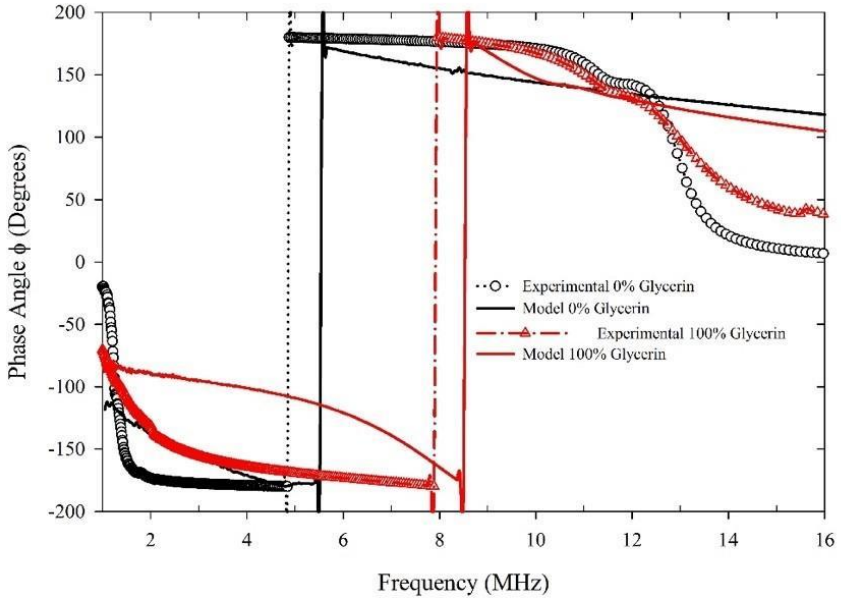

Figure 4.7 Variations in phase shift with frequency for both experimental and simulated results at different concentration of glycerin and water

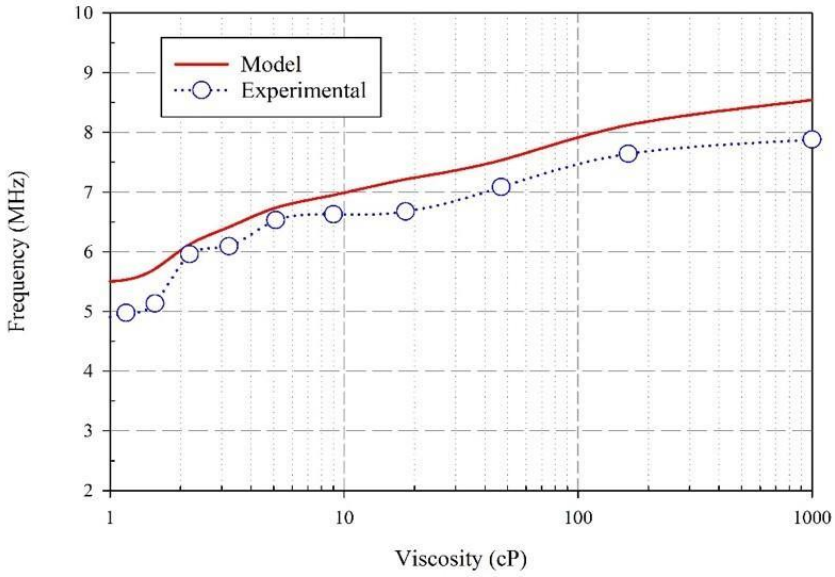

Figure 4.8 Variations in viscosity with resonant frequency for both experimental and modeled results

CHAPTER 5 Conclusions

Non-destructive evaluation techniques applied in a fluid medium can be used to monitor acoustic wave propagations. In addition, fluid properties such as viscosity can be correlated.

In this work, a piezoelectric actuator-sensor pair is immersed into a fluid experimentally and modelled numerically. Numerically, three different geometries with piezoelectric materials are performed to study the sensitivity of the different materials and the different modes of vibration.. Additionally, three different piezoelectric materials (PMN32, PZT5A and PZT4) were assigned in the model. Validating of the numerical model is done by constructing an experimental setup consisting of two circular actuator-sensor pair type PZT 5A immersed into a container filled with fluid (100% water and 100% glycerin); a voltage signal of 0.5 V was then applied to the actuator in the form of a sinusoidal wave with frequency range from 100 Hz to 40 MHz using an impedance analyzer. The experimental results included a measurement of gain for different fluids at different selected distances, and this result was later used to compare it with the numerical results.

The numerical analysis used a two-way Fluid Structure Interaction (FSI) method to enable modelling the interaction between the structure (piezoelectric) pair in this case and the surrounding fluid domain. This method was based on performing harmonic analysis to the actuator under an excitation voltage of (0.5 V) at a frequency range of (100-10000) Hz, and then performing another harmonic acoustic analysis to the fluid domain between the piezoelectric pair by applying the results obtained from the previous harmonic analysis. Finally, another harmonic analysis was performed to the sensor by applying the results obtained from the acoustic harmonic analysis. The results included total deformations and voltages for the actuator-sensor piezoelectric pair for the

three different geometries and the three different materials. Also, the results included acoustic pressure variations between the actuator-sensor pair obtained at different selected distances. The results showed exponential decay between the actuator and sensor pair in the form ($P=P_{\circ} e^{-\alpha x}$), where P is the output pressure, $P_{\circ}$ is the applied pressure on the actuator due to the applied excitation voltage, α is parameter related to the dynamic viscosity, ω is the sound angular frequency, ρ is the fluid density, and V is the speed of sound in the fluid medium. Also, the results showed that maximum acoustic pressure can be obtained by using a square piezoelectric pair and PMN32, but this presents an interesting case for the comparison with other piezoelectric materials. Also, the experimental results showed an exponential decay in the gain between the actuator-sensor pair. This work is important when deciding what optimal geometry and piezoelectric material should be used when designing and fabricating a non-destructive viscosity sensor. Based on the results, the square or rectangle piezoelectric shape is the optimal geometry because it is commercially available, inexpensive and easy to make.

This work also included building a disposable and inexpensive device to monitor the viscosity changes in a fluid as an application of nondestructive evaluation in a fluid. This probe consists of an actuator and a sensor, both made of a commercially available soft piezoelectric material (PZT-5A). It is mainly designed around two constraints, 1) size, designed to fit into a 3 mL vacutainer, and 2) cost: designed to be low-cost and disposable. The operation of the device is based on a tuning fork principle as part of a mechanism for transmitting waves in a fluid medium. The actuator is powered with a sinusoidal signal that vibrates, generating an acoustic wave through a fluid. The sensor detects the produced wave in the liquid. The phase shift between the emitted and detected wave signal was recorded and plotted for different concentrations of glycerin and water. Numerical simulations through a finite element method (FEM) and the ANSYS software were performed.

Acoustic modal and harmonic acoustic analysis results from the simulations predicted the experimental results. The results from the modal analysis showed that the first, second, and third modes of the probe were in the range of 683.9–2358 Hz for air, 499.6–1080.2 Hz for water, and 468.5–625.4 Hz for glycerin. From the harmonic acoustic analysis, the results showed the ultrasonic frequency for phase shift effects ranges from 6 to 9 MHz. These results demonstrated that the natural frequencies of the probe are in the kHz region, and the phase shift frequencies are predicted to be in the high-frequency range.

The results obtained seemed to be directly linked to the (electric) acoustic impedance of the probe in a fluid as observed in the impedance measurements of the actuator and sensor. Results showed a trend: a phase shift increases with the viscosity of the liquid. Furthermore, the results of this work demonstrated that wall interference is not a contributing factor because the distance between the sensor and actuator is minimal. The main contribution of this device to the field of viscosity monitoring, is the utilization of techniques used in structural health monitoring. The developed method, additionally, has many advantages over other devices including size, portability, low cost, minimal liquid sample requirements and is disposable. All these characteristics enable a variety of uses for this method, such as inline monitoring and point-of-care devices. For example, it can be used in medical applications such as monitoring a person in an ambulance who suffers from a chronic disease. The approach and built probe are the initial steps for the development of a robust system. Accuracy and repeatability have not yet been assessed. The device has not yet been tested with non-Newtonian or moving fluids, and those research areas need to be expanded numerically and experimentally. The method may also have other applications, such as acoustic pressure sensors or density monitoring.

CHAPTER 6 Recommendations and Future Work

The recommendations for future work include the following:

- Study the effect of the piezoelectric polarization (i.e., change the orientation of the piezoelectric materials) on the results and compare it with the current results.
- Study the effect of the fluid height level and volume on the results.
- Study the effect of using the two different piezoelectric materials and see the effect on the results.
- Investigate the effect of the temperature on the results, especially given that temperature affects both piezoelectric materials and fluid.

References

[1] S. Her and S. Lin, "Non-destructive Evaluation of Depth of Surface Cracks Using Ultrasonic Frequency Analysis," *Journal of Sensors*, vol. 14, pp. 17146-17158, Sep. 2014.

[2] S. Fateri, P. Lowe, B. Engineer and N. Boulgouris, "Investigation of Ultrasonic Guided Waves Interacting with Piezoelectric Transducers," *Journal of IEEE Sensors*, vol. 15, no. 8, pp. 4319-4328, Aug. 2015.

[3] S. Khante and S. Gedam, "PZT Based Smart Aggregate for Unified Health Monitoring of RC Structures," *Open Journal of Civil Engineering*, vol. 6, no. 1, pp. 42-49, 2016.

[4] A. Katunin, K. Dragan and M. Dziendzikowski, "Damage identification in aircraft composite structures: A case study using various non-destructive testing techniques," *Composite Structures*, vol. 127, pp. 1-9, Sep. 2015.

[5] B. Ren and C. Lissenden, "PVDF Multielement Lamb Wave Sensor for Structural Health Monitoring," *IEEE Trans. Ultrason.*, vol. 63, no. 1, pp. 178-185, Jan. 2016.

[6] C. Willberg, S. Duczek, J. Vivar-Perez and Z. Ahmad, "Simulation Methods for Guided Wave-Based Structural Health Monitoring: A Review," *Applied Mechanics Reviews*, vol. 67, no. 1, p. 010803, Jan. 2015.

[7] R. Takpara, M. Duquennoy, M. Ouaftouh, C. Courtois, F. Jenot and M. Rguiti, "Optimization of PZT ceramic IDT sensors for health monitoring of structures," *Ultrasonic*, vol. 79, pp. 96-104, 2017.

[8] F. Foster, C. Pavlin, K. Harasiewicz, D. Christopher and D. Turnbull, "Advances in ultrasound bio microscopy," *Ultrasound Med Biol.*, pp. 1-27, Jan. 2000.

[9] A. Bucaro, H. Dardy and E. Carome, "Fiber-optic hydrophone," *J. Acoustic. Soc. Amer.*, vol. 62, no. 5, pp. 1302-1304, 1977.

[10] C. Dandridge and K. Kirkendall, "Overview of high performance fibre-optic sensing," *J. Phys. D, Appl. Phys.*, vol. 37, no. 18, pp. R197-R216, 2004.

[11] A. Kersey and A. Culshaw, "Fiber-optic sensing: A historical perspective," *J. Light weight Technol.*, vol. 26, no. 9, pp. 1064-1078, May 2008.

[12] R. Crickmore, "Remotely pumped and interrogated 96 channel fibre-optic hydrophone array," in *In Proc. 16th Opt. Fibre Sensor Conf. Tech.*, Dig., 2003.

[13] P. Dakin, C. Wade and M. Henning, "Novel optical fibre hydrophone array using a single laser source and detector," *Electron. Lett.*, vol. 20, no. 1, pp. 53-54, 1984.

[14] J. Xu, X. Wang, K. L. Cooper and A. Wang, "Miniature all-silica fiber optic pressure and acoustic sensors," *Opt. Lett.*, vol. 30, no. 24, pp. 3269-3271, 2005.

[15] D. Donlagic and E. Cibula, "All-fiber high-sensitivity pressure sensor withSiO2 diaphragm," *Opt. Lett.*, vol. 30, no. 12, pp. 2071-2073, 2005.

[16] O. Kilic, M. Digonnet, G. Kino and O. Solgaard, "External fibre Fabry–P´erot acoustic sensor based on a photonic-crystal mirror," *Meas. Sci.Technol*, vol. 18, no. 10, pp. 3049-3054, 2007.

[17] J. Ma, W. Jin, H. Ho and j. Dai, "High-sensitivity fiber-tip pressure sensor with graphene diaphragm," *Optics Letters,* vol. 37, no. 13, pp. 2494-2495, 2012.

[18] F. Xu, D. Ren, X. Shi, C. Li, W. Lu, L. Lu, L. Lu and B. Yu, "High-sensitivity Fabry–P´erot interferometric pressure sensor based on a nano thick silver diaphragm," *Optics Letters,* vol. 37, no. 2, pp. 133-135, 2012.

[19] G. A. Cranch, G. Flockhart and C. Kirkendall, "Distributed feedback fiber laser strain sensors," *Journal IEEE Sensors,* vol. 8, no. 7, pp. 1161-1172, Jul. 2008.

[20] S. Foster, A. Tikhomirov, M. Milnes, J. V. Velzen and a. G. Hardy, "A fibre laser hydrophone," *Proc. SPIE,* vol. 5855, pp. 627-630, 2005.

[21] W. Zhang, Y. Liu, F. Li and H. Xiao, "Fiber laser hydrophone based on double diaphragms: Theory and experiment," *J. Light weight Technol*, vol. 26, no. 10, pp. 1349-1352, May 2008.

[22] L. Ma, Y. Hu, H. Luo and Z. Hu, "DFB fiber laser hydrophone with flat frequency response and enhanced acoustic pressure sensitivity," *IEEE Photon. Technol. Lett.,* vol. 21, no. 17, pp. 1280-1282, Sep. 2009.

[23] S. Foster et al, "A 16 channel fibre laser sensor array," in *Proc. Austin Conf. Opt. Fiber Technol./Aust. Opt. Soc.*, 2006.

[24] D. Hill, P. Nash, D. Jackson, D. Webb, S. O'Neil, I. Bennion and Z. L., "Fibre laser hydrophone array," in *Proceedings Volume 3860.*, Boston, 1999.

[25] M. Gallo, L. Ferrara, D. Naviglio, "Application of Ultrasound in Food Science and Technology: A Perspective," *Foods,* vol. 164, no. 7, pp. 1-18, 2018.

[26] S. Kumar and D. Mahto, " Recent trends in industrial and other engineering applications of non-destructive testing: a review," *International Journal of Scientific & Engineering Research,* p. 4(9), 2013.

[27] K. Kwong, Y. Lim and W. Liew, "Non-destructive Concrete Strength Evaluation Using PZT Based Surface Wave Propagation Technique – A Comparative Study," in *MATEC Web of conferences,* 2016.

[28] S. Park, C. Yun, Y. Roh and J. Lee, "PZT-based active damage detection techniques for steel bridge components," *Smart Mater. Struct.*, vol. 15, pp. 957-966, 2006.

[29] M. Kishore, D. Park, J. Jeong and J. Kim, "Detection of Deep Subsurface Cracks in Thick Stainless-Steel Plate," *Journal of Magnetics,* vol. 20, no. 3, pp. 312-316, 2015.

[30] F. Song, G. Huang and K. Hudson, "Guided wave propagation in honeycomb sandwich structures using a piezoelectric actuator/sensor system," *Smart Materials and Structures,* vol. 18, pp. 1-8, 2009.

[31] V. Chillara, H. Cho, M. Hasanian and C. Lissenden, "Effect of Load and Temperature Changes on Nonlinear Ultrasonic Measurements: Implications for SHM," 2015.

[32] F. Song, G. Huang, J Kim and S. Haran, "On the study of surface wave propagation in concrete structures using a piezoelectric actuator/sensor system," *Smart Mater. Struct,* vol. 17, pp. 1-8, 2008.

[33] B. Jakoby and M. Vellekoop, "Physical Sensors for Liquid Properties," *IEEE sensors Journal,* vol. 11, no. 12, pp. 3076-3085, 2011.

[34] A. Anderson, B. Bruno and L. Smith, Viscosity measurement, 2014, pp. 1-28.

[35] Z. Zhu, Z. Zhong and J. Zhe, "Lubricating oil conditioning sensors for online machine health monitoring–A review," *Tribology international*, vol. 109, pp. 473-484, 2017.

[36] W. Gao, Y. Nyein, Z. Shahpar, H. Fahad, K. Chen, S. Emaminejad, Y. Gao, L. Tai, H. Ota, E. Wu, J. Bullock, Y. Zeng, D. Lien and J. A., "Wearable Microsensor Array for Multiplexed Heavy Metal Monitoring of Body Fluids," *ACS Sens.*, vol. 1, no. 7, pp. 866-874, 2016.

[37] F. Irgens, Rheology and Non-Newtonian fluids., Springer, 2014.

[38] B. Nikolic, B. Kegl, S. Markovic and M. Mitrovic, "Determining the speed of sound, density and bulk modulus of rapeseed oil, biodiesel and diesel fuel," *Thermal sci*, vol. 16, no. 2, pp. 505-514, 2012.

[39] A. Lopes, M. Talavera-Prieto, A. Ferreira, J. Santos, M. Santos and A. Portugal, "Speed of sound in pure fatty acid methyl esters and biodiesel fuels," *Fuel*, vol. 116, pp. 242-254, 2014.

[40] E. Baltasar, M. Taravillo, V. Baonza, P. Sanz and B. Guignon, "Speed of Sound in Liquid Water from (253.15 to 348.15) K and Pressures from (0.1 to 700) MPa," *Journal of Chemical & Engineering Data*, vol. 56, no. 12, pp. 4800-4807, 2011.

[41] S. Vance and J. Brown, "Sound velocities and thermodynamic properties of water to 700 MPa and −10 to 100 °C," *The Journal of the Acoustical Society of America*, vol. 127, no. 1, pp. 174-180, January 2010.

[42] E. Jeon, W. Kim, I. Kim and H. Park, "Measurement of Sound Speed Following the Fluid Temperature Using Acoustic Inspection Device," *비파괴검사학회지,* vol. 30, no. 3, pp. 207-211, 2010.

[43] D. Xiao, M. Deng, Q. Pan, D. Sheng and B. Yang, "Measurement of Ultrasonic Transducer Sensitivity," in *International Conference on Mechatronics and Automation*, Chengdu, 2012.

[44] S. Banerjee, T. Kundu and D. Placko, "Ultrasonic Field Modeling in Multilayered Fluid Structures Using the Distributed Point Source Method Technique," *Transactions of the ASME,* vol. 73, pp. 598-609, 2006.

[45] D. Mark, S. Haeberle, F. Von Stettenzab and R. Zengerle, "Microfluidic lab-on-a-chip platforms: requirements, characteristics and applications," *Chemical Society Reviews,* vol. 39, pp. 1153-1182, 2010.

[46] S. Gopinath, T. Tang, M. Citartan, Y. Chen and T. Lakshmipriya, "Current aspects in immunosensors," *Biosensors and Bioelectronics,* vol. 57, pp. 292-302, July 2014.

[47] Y. Fu, J. Luo, N. Nguyen, A. Walton, A. Flewitt, X. Zu, Y. Li, G. McHale and A. Matthews, "Advances in piezoelectric thin films for acoustic biosensors, acoustofluidics and lab-on-chip applications," *Prog. Mater. Sci.*, vol. 89, pp. 31-91, 2017.

[48] R. Shilton, M. Tan, L. Yeo and J. Friend, "Particle concentration and mixing in micro drops driven by focused surface acoustic waves.," *J. Appl. Phys.*, vol. 104, pp. 1-10, 2008.

[49] X. Ding, S. Lin, B. Kiraly, H. Yue, S. Li, J. Shi, S. Benkovic and T. Huang, "On-chip manipulation of single microparticles, cells, and organisms using surface acoustic waves," *Proc. Natl. Acad.*, vol. 109, pp. 11105-11109, 2012.

[50] N. Orloff, J. Dennis, M. Cecchini, E. Schonbrun, E. Rocas, Y. Wang, D. Novotny, R. Simmonds, J. Moreland, I. Takeuchi and e. al., "Manipulating particle trajectories with phase-control in surface acoustic wave microfluidics.," *Bio microfluidics*, vol. 5, pp. 044107-044107, 2011.

[51] M. Demori, M. Baù, M. Ferrari and V. Ferrari, "Piezoelectric Actuators for In-Liquid Particle Manipulation in Microfluidic Applications," in *Euro sensors 2017 Conference*, Paris, 2017.

[52] S. Antlinger, R. Clara, S. Beigelbeck, F. Cerimovic, Keplinger and B. Jakoby, "Sensing the characteristic acoustic impedance of a fluid utilizing acoustic pressure waves," *Sensors and Actuators A: Physical*, vol. 186, pp. 94-99, 2012.

[53] H. Antlinger, S. Clara, R. Beigelbeck, S. Cerimovic, F. Keplinger and B. Jakoby, "Utilizing acoustic pressure waves for sensing fluid properties," in *Procedia Engineering*, 2011.

[54] H. Antlinger, R. Beigelbeck, S. Clara, S. Cerimovic, F. Keplinger and B. Jakoby, "Investigation and Modeling of an Acoustoelectric Sensor Setup for the Determination of the Longitudinal Viscosity," *IEEE Trans. Ultrason., Ferroelect. Freq. Contr.*, vol. 63, no. 12, pp. 2187-2197, 2016.

[55] H. Antlinger, S. Clara, R. Beigelbeck, S. Cerimovic, F. Keplinger and B. Jakoby, "A Differential Pressure Wave-Based Sensor Setup for the Acoustic Viscosity of Liquids," *IEEE Sensors Journal*, vol. 16, no. 21, pp. 7609-7619, 2016.

[56] R. Waxman, U. Erturun and K. Mossi, "Feasibility of using piezoelectric probes to measure viscosity in newtonian fluids," in *ASME 2010 Conference on Smart materials*, 2010.

[57] A. Abdulkareem, U. Erturun and K. Mossi, "Non-destructive Evaluation Device for Monitoring Fluid Viscosity," *sensors*, vol. 20, no. 1657, pp. 1 - 14, 2020.

[58] G. Hou, J. Wang and A. Layton, "Numerical Methods for Fluid-Structure Interaction -A review," *communications in computational physics*, vol. 12, no. 2, pp. 337-377, 2012.

[59] S. Chhakrabartic, Numerical Models in Fluid Structure Interaction, Advances in Fluid Mechanics, vol. 42, WIT press., 2005.

[60] E. Dowell and K. Hall, "Modeling of fluid-structure interaction," *Annual Review of Fluid Mechanics*, vol. 33, pp. 445-490, 2001.

[61] H. Morand and R. Ohayon, Fluid-Structure Interaction: Applied Numerical Methods, Wiley, 1995.

[62] W. Liu, D. Kim and S. Tang, "Mathematical foundations of the immersed finite element method," *Computational Mechanics*, vol. 39, pp. 211-222, 2006.

[63] W. Hasse, "Unsteady Aerodynamics Including Fluid/Structure Interaction," *Air and Space Europe*, vol. 3, pp. 83-86, 2001.

[64] L. Zhang and M. Gay, "Immersed finite element method for fluid-structure interactions," *Journal of Fluids and Structures,* vol. 23, no. 6, pp. 839-857, 2007.

[65] G. Kaligzin and G. Iaccarino, "Toward immersed boundary simulation of high Reynolds Number flows," in *Annual Research Briefs, Center for Turbulence Research*, Stanford University, 2003.

[66] J. Yang and E. Balaras, "An embedded-boundary formulation for large-eddy simulation of turbulent flows interacting with moving boundaries," *Journal of Computational Physics,* vol. 215, pp. 12-40, 2006.

[67] E. Fadlun, R. Verzicco, P. Orlandi and J. Mohd-Yusof, "Combined immersed-boundary finite-difference methods for three-dimensional complex flow simulations," *Journal of Computational Physics,* vol. 161, pp. 35-60, 2000.

[68] H. Udaykumar, W. Shyy and M. Rao, "A mixed Eulerian-Lagrangian Method for fluid flows with complex and moving boundaries," I*nternational Journal for Numerical Methods in Fluids,* vol. 22, pp. 691-705, 1996.

[69] H. Udaykumar, R. Mittal, P. Rampunggoon and A. Khanna, "A sharp interface Cartesian Grid method for simulating flows with complex moving boundaries," *Journal of Computational Physics,* vol. 174, pp. 345-380, 2001.

[70] J. Hoburg and J. Melcher, "Internal electrohydrodynamic instability and mixing of fluids with orthogonal field and conductivity gradients," *Journal of Fluid Mechanics,* vol. 73, pp. 333-351, 1976.

[71] B. Griffith and C. Peskin, "On the order of accuracy of the immersed boundary method: Higher order convergence rates for sufficiently smooth problems," *Journal of Computational Physics*, vol. 208, pp. 75-105, 2005.

[72] P. Chen, Z. Yulong and L. Yiyao, "Fluid Structure Interaction Analysis and Simulation of Micromachined cantilever-based flow sensor," in *Conference on Nano/Micro Engineered and Molecular Systems*, Hawaii, USA, 2014.

[73] E. Reichela, C. Rieschb, F. Keplingerb and B. Jakobya, "Modeling of the fluid-structure interaction in a fluidic sensor cell," *Sensors and Actuators A: Physical*, vol. 156, pp. 222-228, 2009.

[74] Z. Bofang, The Finite Element Method: Fundamentals and Applications in Civil, Hydraulic, Mechanical and Aeronautical Engineering, Wiley, 2018.

[75] L. Kinsler, A. Frey, A. Coppens and A. Sanders, Fundamentals of Acoustics, New York: John Wiley and Sons, 1999.

[76] W. Graebel, Advanced Fluid Mechanics, Burlington, MA: Elsevier, 2007.

[77] K. Bathe, Finite element procedures., Englewood: Prentice-Hall, 1996.

[78] O. Zienkiewicz and R. Newton, "Coupled vibrations of a structure submerged in a compressible fluid," in *Symposium on Finite Element*, University of Stuttgart, 1969.

[79] A. Craggs, "Finite element model for acoustically lined small rooms.," *J Sound Vibrat*, vol. 108, no. 2, pp. 327-373, 1986.

[80] C. Rajakumar and A. Ali, "Acoustic boundary element eigenproblem with sound absorption and its solution using lanczos algorithm," *J Numer Meth Eng*, vol. 36, no. 23, pp. 3957-3972, 1993.

[81] D. Woyjak, "Acoustic and fluid structure interaction, a revision 5.0," Swanson Analysis Systems, Inc, Swanson Analysis Systems, Inc, 1992.

[82] J. Gere, Mechanics of Materials, Thomson Learning Inc:Belmont: CA, 2004.

[83] A. Nechibvute, A. Chawanda and P. Luhanga, "Finite Element Modeling of a Piezoelectric Composite Beam and Comparative Performance Study of Piezoelectric Materials for Voltage Generation," *ISRN Materials Science*, vol. 2012, pp. 1-11, 2012.

[84] "ANSYS Mechanical APDL Modeling and Meshing Guide," Canonsburg, PA, 2010.

[85] B. Jakoby and M. Vellekoop, "Physical sensors for liquid properties," *IEEE Sensors Journal, vol.* 11, no. 12, pp. 3076-3085, 2011.

[86] M. Youssry, N. Belmiloud, B. Caillard, C. Ayela, C. Pellet and I. Dufour, "A straightforward determination of fluid viscosity and density using microcantilevers: From experimental data to analytical expressions," *Sensors and Actuators A: Physical*, vol. 172, no. 1, pp. 40-46, 2011.

[87] X. Zhu, C. Zhong and J. Zhe, "Lubricating oil conditioning sensors for online machine health monitoring–A review," *Tribology International*, vol. 109, pp. 473-484, 2017.

[88] J. Toledo, F. Jiménez-Márquez, J. Úbeda, V. Ruiz-Díez, G. Pfusterschmied, U. Schmid and J. Sánchez-Rojas, "Piezoelectric MEMS resonators for monitoring grape must fermentation," in *Journal of Physics: Conference Series*, Corl,Irland, 2016.

[89] J. Muñoz, J. Ancheyta and L. Castañeda, "Required Viscosity Values to Ensure Proper Transportation of Crude Oil by Pipeline," *Energy Fuels*, vol. 30, pp. 8850 - 8854, 2016.

[90] H. Wu, G. Zhao, H. Zu, J. Wang and Q. Wang, "Real-time monitoring of platelet activation using quartz thickness-shear mode resonator sensors.," *Biophysical Journal*, vol. 110, pp. 669-679, 2016.

[91] A. Anderson, B. Bruno and L. Smith, "Viscosity measurement," in *Volume I. Materials and Engineering Mechanics*, Schenectady, New york, 2014, pp. 1-28.

[92] H. Antlinger, S. Clara, R. Beigelbeck, S. Cerimovic, F. Keplinger and B. Jakoby, "Utilizing acoustic pressure waves for sensing fluid properties," in *Procedia Enginering*, 2014.

[93] L. Zhao, Y. Hu, T. Wang, J. Ding, X. Liu, Y. Zhao and Z. Jiang, "A MEMS resonant sensor to measure fluid density and viscosity under flexural and torsional vibrating modes," *Journal of sensors*, vol. 16, no. 6, pp. 1-15, 2016.

[94] J. Ma, X. Huang, H. Bae, Y. Zheng, C. Liu, M. Zhao and M. Yu, "Liquid viscosity measurement using a vibrating flexure hinged structure and a fiber-optic sensor," *IEEE journal of sensor*, vol. 16, pp. 5249 - 5258, 2016.

[95] Y. Hongbin, L. Liang and A. Yuandong, "Capacitive micromachined ultrasonic transducer (CMUT) based micro viscosity sensor," *Sensors and Actuators B: Chemical*, vol. 227, pp. 346 - 351, 2016.

[96] E. Nwankwo and C. Durning, "Fluid property investigation by impedance characterization of quartz crystal resonators: Part I: Methodology, crystal screening, and Newtonian fluids," *Sensors and Acuators A: Physical*, vol. 72, no. 2, pp. 99-109, 1999.

[97] L. Markova, V. Makarenko, M. Semenyuk and A. Zozulya, "In-line monitoring of the viscosity of lubricating oils," *Journal of frication and wear*, vol. 31, pp. 433 - 442, 2010.

[98] C. Zhang, H. Zhang and S. Kaluvan, "PZN-PT based smart probe for high temperature fluid viscosity measurements," *Measurement*, vol. 94, pp. 753 - 758, 2016.

[99] F. Yan and H. Chan, "Analytical model of piezoelectric cantilever as rheological sensor," *Phys. B Condens. Matter*, vol. 406, pp. 3605 - 3608, 2011.

[100] F. Ju and S. Ling, "Sensing fluid viscosity and density through mechanical impedance measurement using a whisker transducer," *Measurement Science and Technology*, p. 24, 2013.

[101] A. Goodwin, A. Fitt, K. Ronaldson and W. Wakeham, "A vibrating plate fabricated by the methods of microelectromechanical systems (MEMS) for the simultaneous measurement of density and viscosity:Results for argon at temperatures between 323 and 423K at pressures up to 68 MPa.," *International Journal of Thermophysics*, vol. 27, pp. 1650 - 1676, 2006.

[102] I. Etchart, H. Chen, P. Dryden, J. Jundt, C. Harrison, K. Hsu, F. Marty and B. Mercier, "MEMS sensors for density–viscosity sensing in a low-flow microfluidic environment," *Sensors and Actuators A: Physical*, vol. 141, no. 2, pp. 266 - 275, 2008.

[103] P. Purohit, Y. Yadav and S. Jain, "A study of determination of dynamic viscosity in liquids using radial mode piezo-resonator," *Ferroelectrics*, vol. 519, pp. 236 - 240, 2017.

[104] J. Yan, W. Wright, J. O'Mahony, Y. Roos, E. Cuijpers and S. Van Ruth, "sound approach: Exploring a rapid and non-destructive ultrasonic pulse echo system for vegetable oils characterization," *Food Research International*, vol. 125, pp. 1 - 9, 2019.

[105] G. Pfusterschmied, M. Kucera, C. Weinmann, M. Schneider, A. Bittner, J. Sánchez-Rojas and U. Schmid, "Two-step procedure for multi-mode MEMS resonator-based sensing of fluid properties," in *2017 IEEE 30th International Conference on Micro Electro Mechanical Systems (MEMS)*, Las Vegas, NV, 2017.

[106] J. Toledo, V. Ruiz-Díez, G. Pfusterschmied, U. Schmid and J. Sánchez-Rojas, "Characterization of oscillator circuits for monitoring the density-viscosity of liquids by means of piezoelectric MEMS microresonators," in *Smart Sensors, Actuators, and MEMS VIII.; International Society for Optics and Photonics*, Barcelona, Spain, 2017.

[107] J. Toledo, V. Ruiz-Díez, G. Pfusterschmied, U. Schmid and J. Sánchez-Rojas, "Flow-through sensor based on piezoelectric MEMS resonator for the in-line monitoring of wine fermentation," *Sensors and Actuators B: Chemical*, vol. 254, pp. 291 - 298, 2018.

[108] T. Nguyen, M. Nguyen, H. Takahashi, K. Matsumoto and I. Shimoyama, "Viscosity measurement based on the tapping-induced free vibration of sessile droplets using MEMS-based piezoresistive cantilevers," *Lab Chip*, vol. 15, pp. 3670 - 3676, 2015.

[109] R. Abdolvand, B. Bahreyni, J. Lee and F. Nabki, " Micromachined resonators: A review," *Micromachines*, vol. 7, no. 9, pp. 1-56, 2016.

[110] Y. Xin, H. Sun, H. Tian, C. Guo, X. Li, S. Wang and C. Wang, "The use of polyvinylidene fluoride (PVDF) films as sensors for vibration measurement: A brief review," *Ferroelectrics*, vol. 502, pp. 28 - 42, 2016.

[111] M. Prek, "Analysis of wave propagation in fluid-filled viscoelastic pipes," *Mechanical Systems and Singal Processing*, vol. 21, no. 4, pp. 1907 - 1916, 2007.

[112] S. Association, "Glycerin: An overview," Terms Tech Data Prop. Perform, 1990.

Appendix A: Piezoelectric Materials Properties

Relative permittivity (ε_r)

PMN32

$$\begin{bmatrix} 3309 & 0 & 0 \\ 0 & 3909 & 0 \\ 0 & 0 & 1264 \end{bmatrix}$$

PZT-5A

$$\begin{bmatrix} 919.1 & 0 & 0 \\ 0 & 919.1 & 0 \\ 0 & 0 & 826.16 \end{bmatrix}$$

PZT-4

$$\begin{bmatrix} 762.5 & 0 & 0 \\ 0 & 762.5 & 0 \\ 0 & 0 & 663.2 \end{bmatrix}$$

Coupling matrix (e), C/m^2

PMN32

$$\begin{bmatrix} 0 & 0 & 25.68634 \\ 0 & 0 & 13.57143 \\ 0 & 0 & 13.57143 \\ 0 & 0 & 0 \\ 0 & -3.7795 & 0 \\ -3.7795 & 0 & 0 \end{bmatrix}$$

PZT-5A

$$\begin{bmatrix} 0 & 0 & 15.7835 \\ 0 & 0 & 12.2947 \\ 0 & 0 & 12.2947 \\ 0 & 0 & 0 \\ 0 & -5.35116 & 0 \\ -5.35116 & 0 & 0 \end{bmatrix}$$

PZT-4

$$\begin{bmatrix} 0 & 0 & 15.0804 \\ 0 & 0 & 12.7179 \\ 0 & 0 & 12.7179 \\ 0 & 0 & 0 \\ 0 & -5.20279 & 0 \\ -5.20279 & 0 & 0 \end{bmatrix}$$

Elasticity matrix (C_E) $\times 10^{10}$ Pa

PMN32

$$[C] = \begin{pmatrix} 13.3 & 9.85 & 9.63 & 0 & 0 & 0 \\ 9.85 & 13.3 & 9.63 & 0 & 0 & 0 \\ 9.63 & 9.63 & 10.2 & 0 & 0 & 0 \\ 0 & 0 & 0 & 7.14 & 0 & 0 \\ 0 & 0 & 0 & 0 & 7.14 & 0 \\ 0 & 0 & 0 & 0 & 0 & 6.67 \end{pmatrix}$$

PZT-5A

$$[C] = \begin{pmatrix} 12.0346 & 7.51791 & 7.50901 & 0 & 0 & 0 \\ 7.5191 & 12.0346 & 7.50901 & 0 & 0 & 0 \\ 9.63 & 7.50901 & 11.0867 & 0 & 0 & 0 \\ 0 & 0 & 0 & 2.10526 & 0 & 0 \\ 0 & 0 & 0 & 0 & 2.10526 & 0 \\ 0 & 0 & 0 & 0 & 0 & 2.25734 \end{pmatrix}$$

PZT-4

$$[C] = \begin{pmatrix} 13.8999 & 7.78366 & 7.42836 & 0 & 0 & 0 \\ 7.78366 & 13.8999 & 7.42836 & 0 & 0 & 0 \\ 7.42836 & 7.42836 & 11.7436 & 0 & 0 & 0 \\ 0 & 0 & 0 & 2.564 & 0 & 0 \\ 0 & 0 & 0 & 0 & 2.5641 & 0 \\ 0 & 0 & 0 & 0 & 0 & 3.0581 \end{pmatrix}$$

Appendix B: Steps for modeling Fluid - Structural Interaction (FSI) for the actuator – sensor pair immersed in a fluid.

The following steps show the modelling of the FSI for the actuator/sensor PZT pair:

1- Import the assembly, which includes actuator/sensor pair, plastic holders and fluid domain, files from SolidWork with an extension of (*. xt) or (*.igs) to ANSYS workbench as shown in Figure (B-1).

2- Assign the material properties from table (2.1) for the plastic holders and from Appendix (A) for the piezoelectric materials.

3- Create a local coordinate system for both actuator and sensor PZT from a global coordinate system. Assign them in step2 by using cylindrical coordinate systems for the circular PZT pair and cartesian coordinate system for the square and triangular PZT.

4- Assign the mesh configuration for both PZT pair and fluid domain.

5- Perform the harmonic acoustics analysis by setting the frequency range (100 Hz – 10 KHz).

6- Create the acoustic region by selecting the fluid domain.

7- Create the structure region by selecting the actuator – sensor PZT pair.

8- Create the radiation boundary by selecting the faces of the fluid domain.

9- Create the PZT bodies for both sensor and actuator and assign their properties from Appendix A for the relative permittivity and coupling matrix. Assign the polarization axis in the z-direction, in this case.

10- Create a voltage body and assign it as an excitation voltage. Set a voltage of v =0.5 V and apply it to the face of the actuator.

11- Create another voltage body, assign it as a ground voltage of v =0 V and apply it to the other face of the actuator and one face of the sensor.

12- Create a voltage coupling body and apply it to the other face of the sensor.

13- Apply a constraint to the plastic holders.

14- Run the model and find the acoustic pressure between the sensor actuator pair, total deformation on the sensor and actuator, and voltage on the actuator and sensor.

15- Repeat the steps from 2-13 for other PZT pair types.

The steps from (2-13) can be seen in figure (B – 2)

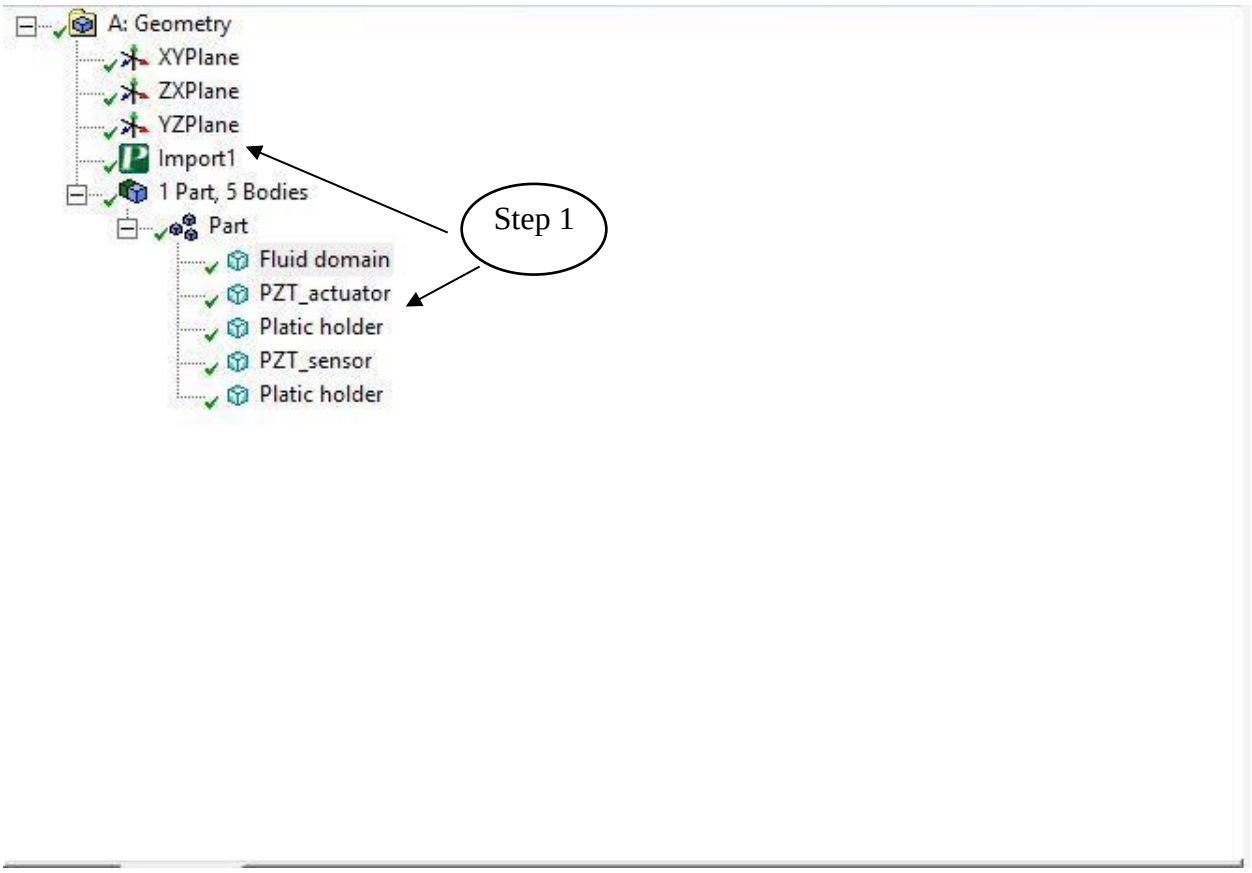

Figure B.1 Import Assembly from Solidworks® software

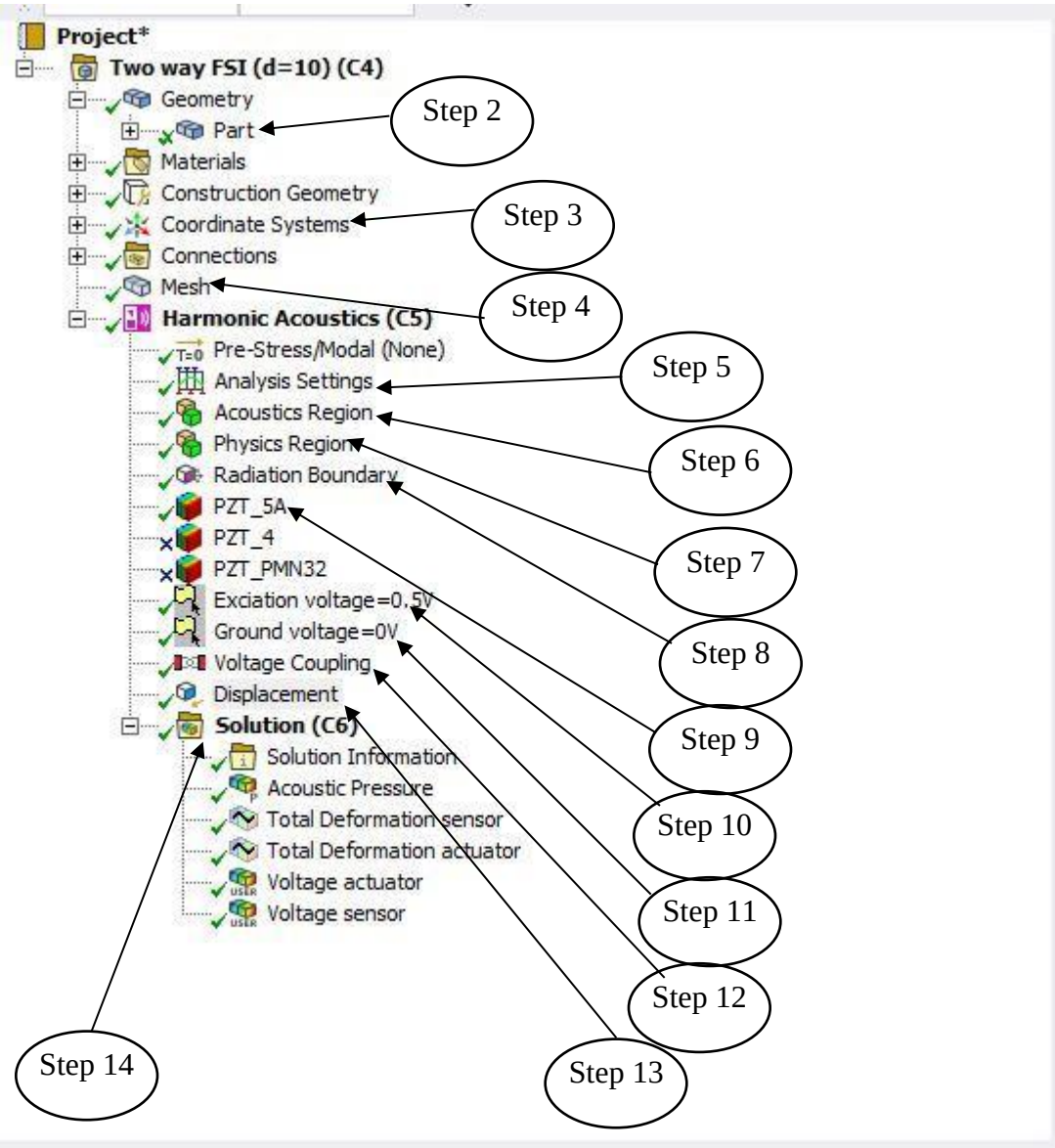

Figure B.2 Main steps for Two - way Fluid Structure Interaction (FSI) modelling

Appendix C: Acoustic pressure variations vs. distance for different geometries

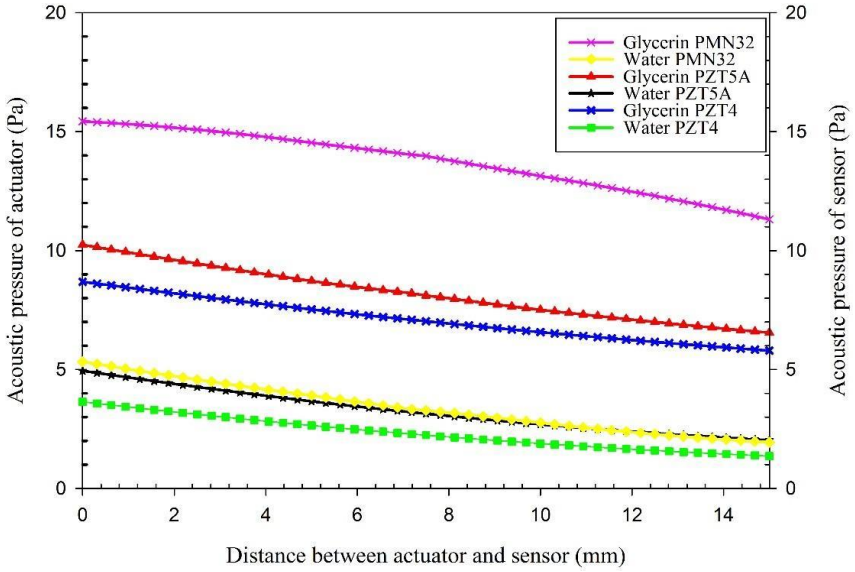

Figure C.1 Acoustic pressure variations vs distance (15mm) for square actuator/sensor PZT pair made of PMN32, PZT4, and PZT5A; immersed in 100 % glycerin and 100 %water

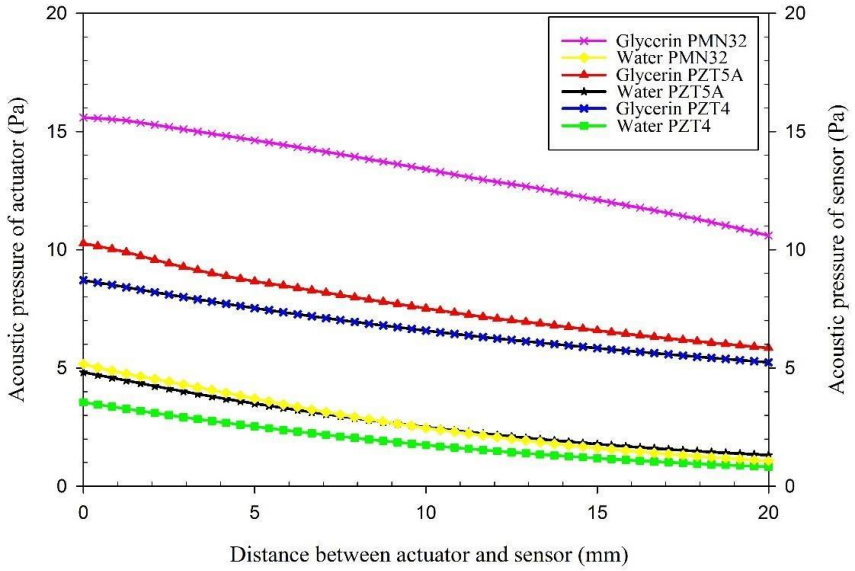

Figure C.2 Acoustic pressure variations vs distance (20 mm) for square actuator/sensor PZT pair made of PMN32, PZT4, and PZT5A; immersed in 100 % glycerin and 100 %water

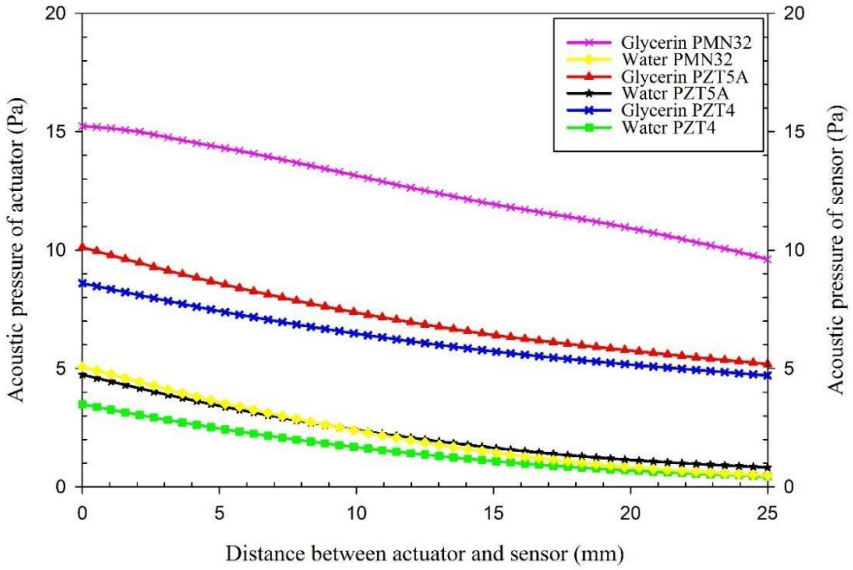

Figure C.3 Acoustic pressure variations vs distance (25mm) for square actuator/sensor PZT pair made of PMN32, PZT4, and PZT5A; immersed in 100 % glycerin and 100 %water

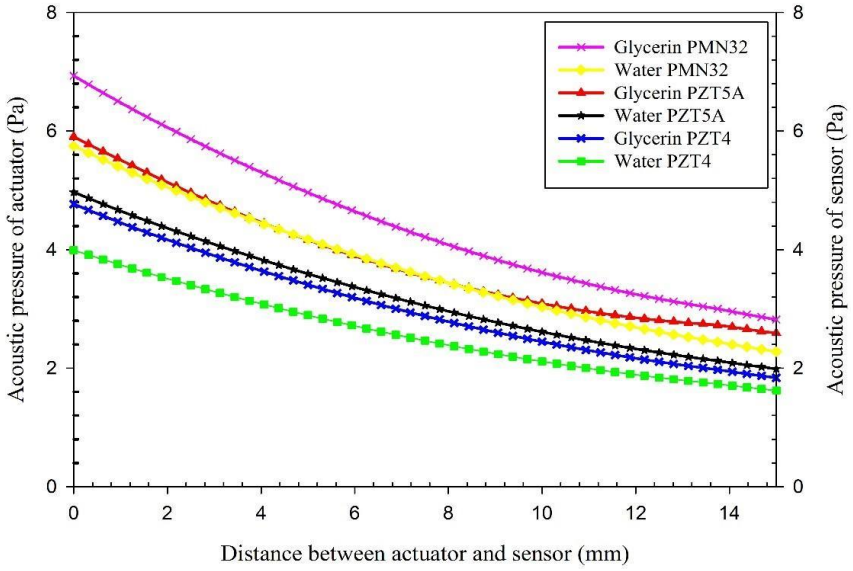

Figure C.4 Acoustic pressure variations vs distance (15mm) for circle actuator/sensor PZT pair made of PMN32, PZT4, and PZT5A; immersed in 100 % glycerin and 100 %water.

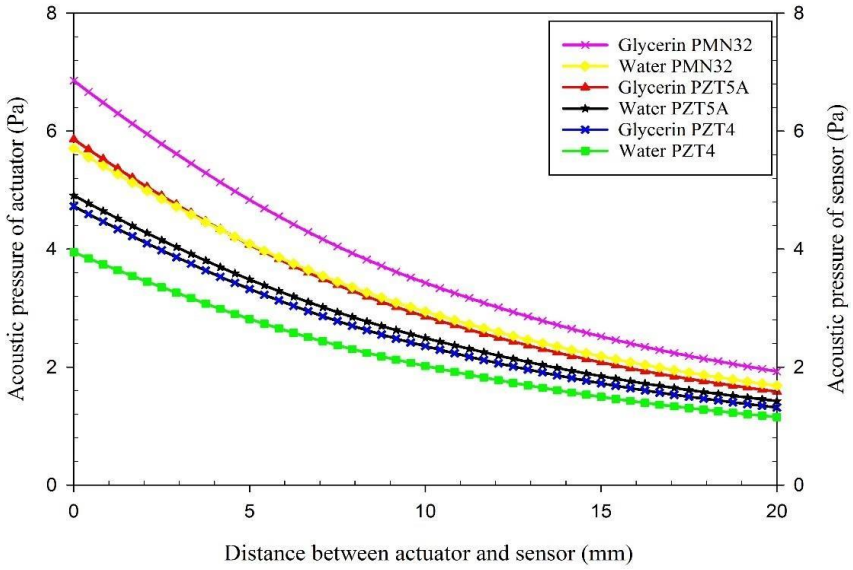

Figure C.5 Acoustic pressure variations vs distance (20 mm) for circle actuator/sensor PZT pair made of PMN32, PZT4, and PZT5A; immersed in 100 % glycerin and 100 %water

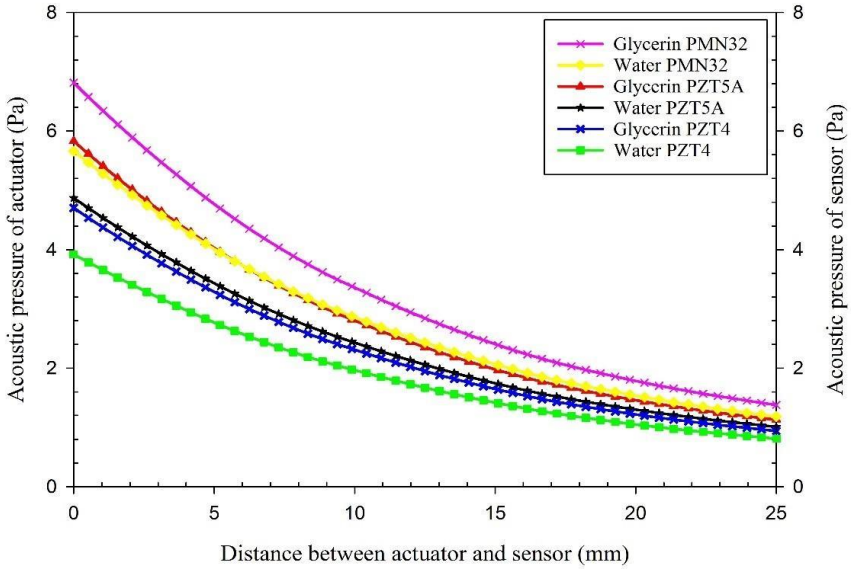

Figure C.6 Acoustic pressure variations vs distance (25 mm) for circle actuator/sensor PZT pair made of PMN32, PZT4, and PZT5A; immersed in 100 % glycerin and 100 %water

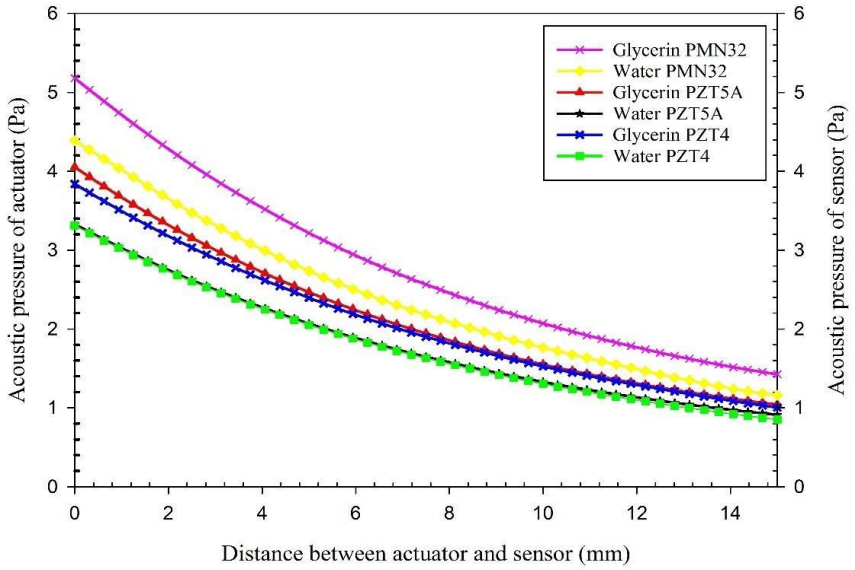

Figure C.7 Acoustic pressure variations vs distance (15 mm) for triangular actuator/sensor PZT pair made of PMN32, PZT4, and PZT5A; immersed in 100 % glycerin and 100 %water

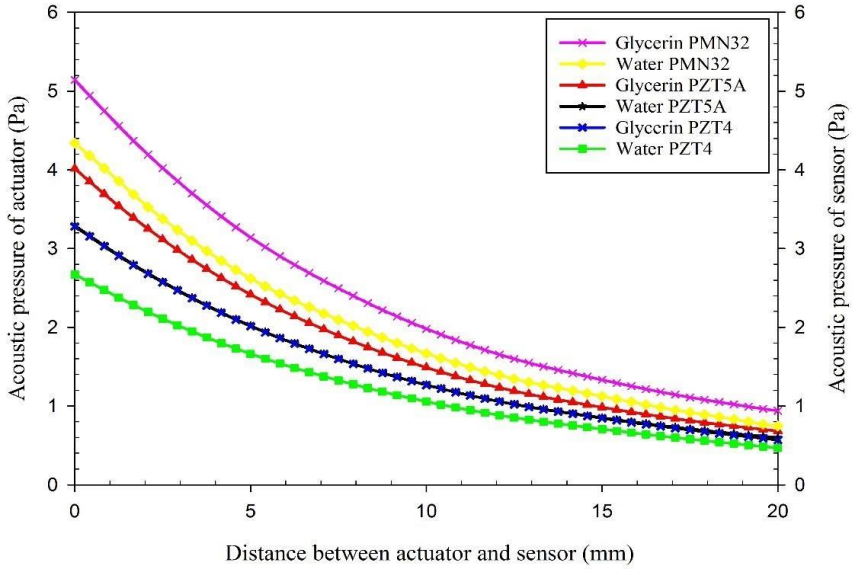

Figure C.8 Acoustic pressure variations vs distance (20 mm) for triangular actuator/sensor PZT pair made of PMN32, PZT4, and PZT5A; immersed in 100 % glycerin and 100 % water

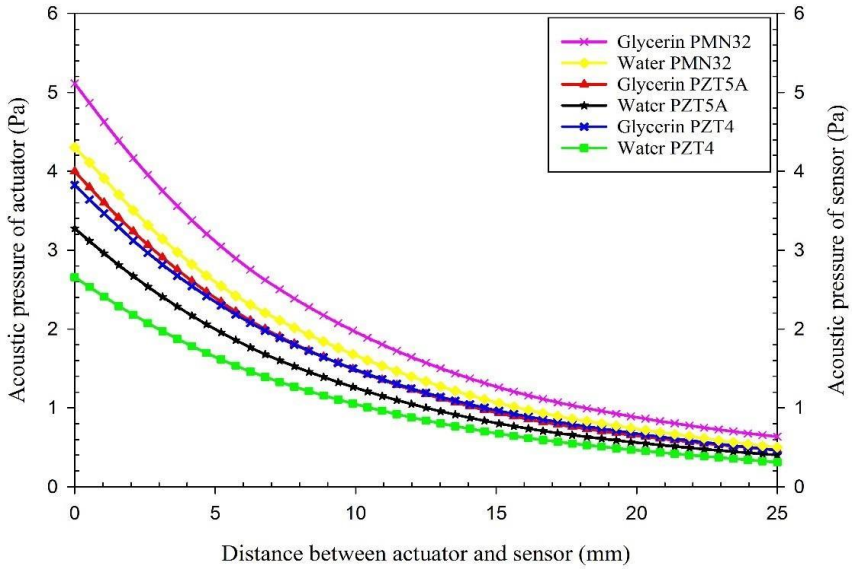

Figure C.9 Acoustic pressure variations vs distance (25 mm) for triangular actuator/sensor PZT pair made of PMN32, PZT4, and PZT5A; immersed in 100 % glycerin and 100 % water

Appendix D: Acoustic pressure variations vs distance for different PZT materials

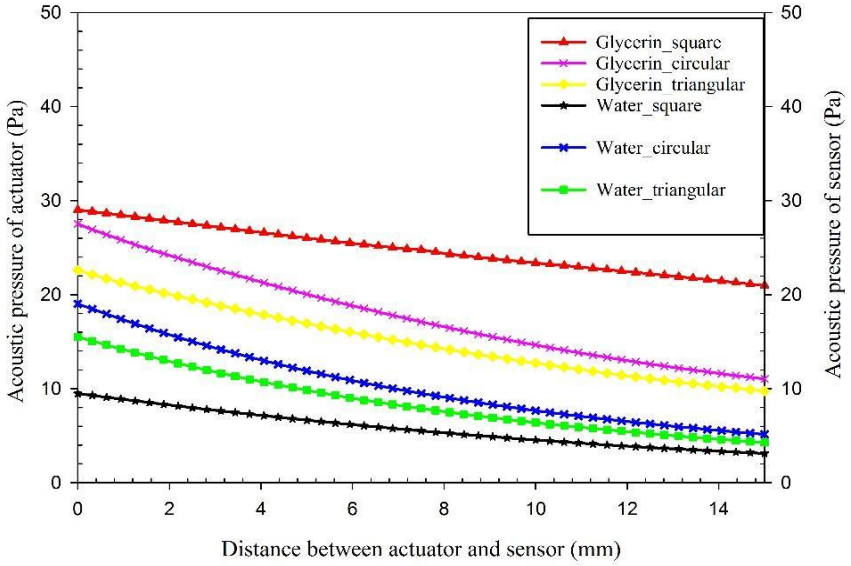

Figure D.1 Acoustic pressure variations vs distance (15 mm) for actuator/sensor PZT pair for different geometries made of PMN32; immersed in 100 % glycerin and 100 % water

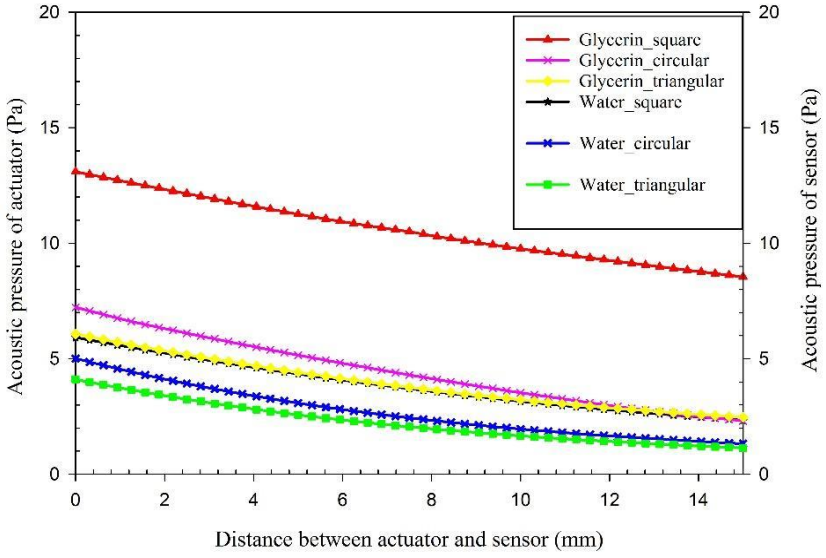

Figure D.2 Acoustic pressure variations vs distance (15 mm) for actuator/sensor PZT pair for different geometries made of PZT 5A; immersed in 100 % glycerin and 100 % water

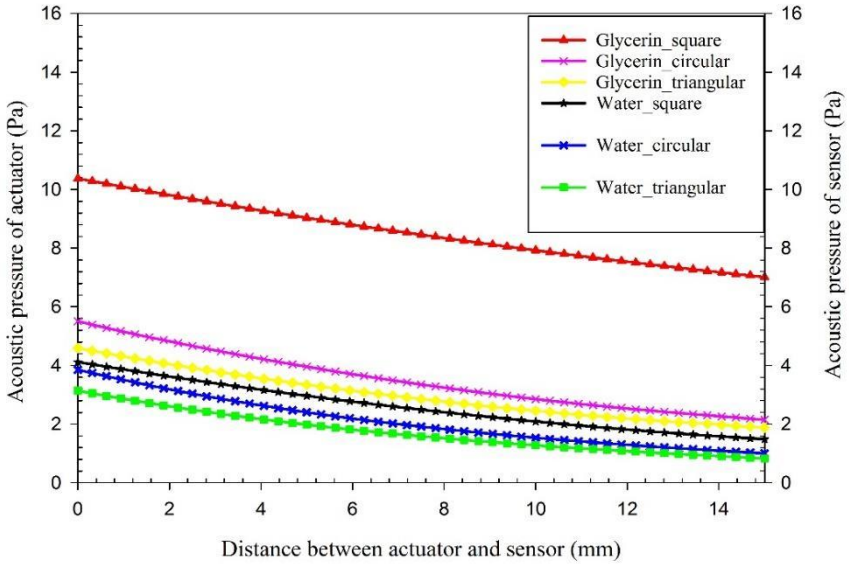

Figure D.3 Acoustic pressure variations vs distance (15 mm) for actuator/sensor PZT pair for different geometries made of PZT 4; immersed in 100 % glycerin and 100 % water

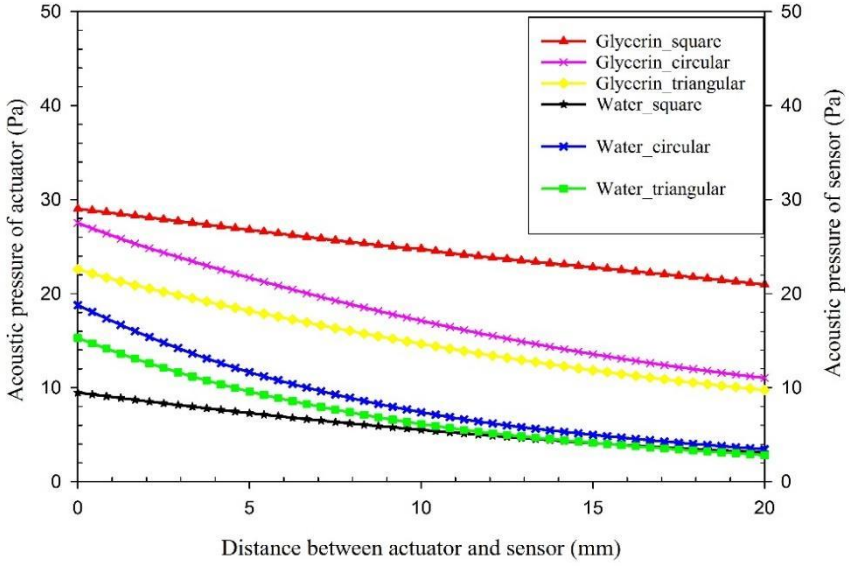

Figure D.4 Acoustic pressure variations vs distance (20 mm) for actuator/sensor PZT pair for different geometries made of PMN32; immersed in 100 % glycerin and 100 % water

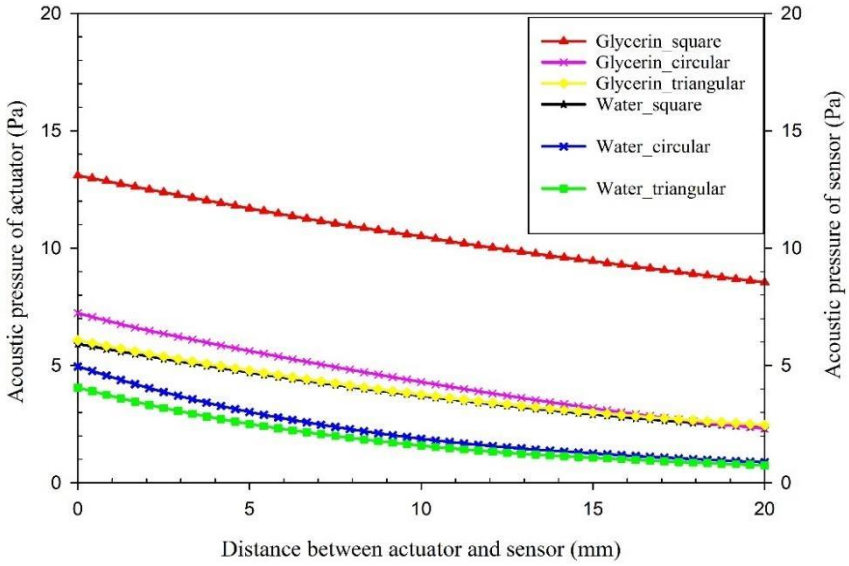

Figure D.5 Acoustic pressure variations vs distance (20 mm) for actuator/sensor PZT pair for different geometries made of PZT 5A; immersed in 100 % glycerin and 100 % water

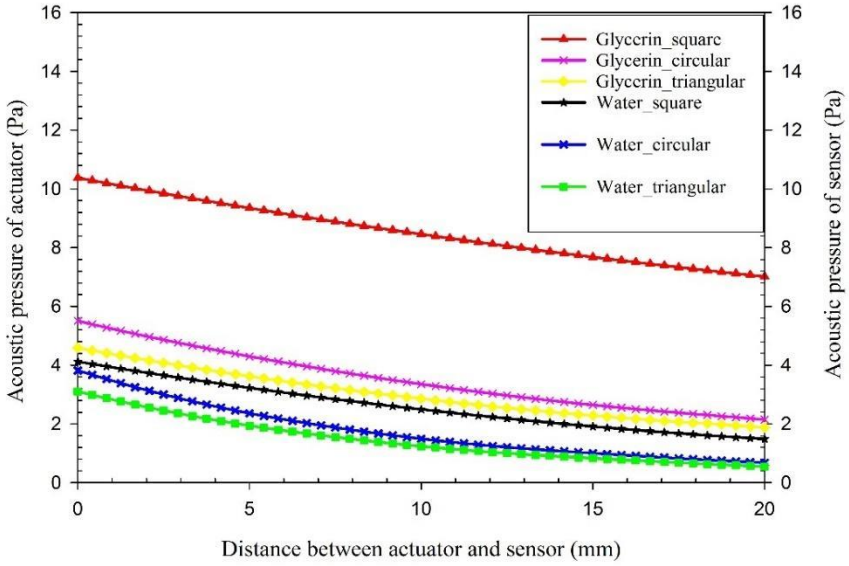

Figure D.6 Acoustic pressure variations vs distance (20 mm) for actuator/sensor PZT pair for different geometries made of PZT 4; immersed in 100 % glycerin and 100 % water

Publications

1. Abdulkareem, A., U. Erturun and K. Mossi (2020). "Non-Destructive Evaluation Device for Monitoring Fluid Viscosity." Sensors 20(6): 14..

2. Ahmed Abdulkareem, Ugur Erturun and Karla Mossi," Investigation of wave propagation due to Non-destructive Evaluation technique for Newtonian fluids". In preparation